EUROPEAN RESPIRATORY *journal*

FLAGSHIP SCIENTIFIC JOURNAL OF ERS

Early View

Original research article

Fibroblasts positive for meflin have anti-fibrotic property in pulmonary fibrosis

Yoshio Nakahara, Naozumi Hashimoto, Koji Sakamoto, Atsushi Enomoto, Taylor S. Adams, Toyoharu Yokoi, Norihito Omote, Sergio Poli, Akira Ando, Keiko Wakahara, Atsushi Suzuki, Masahide Inoue, Akitoshi Hara, Yasuyuki Mizutani, Kazuyoshi Imaizumi, Tsutomu Kawabe, Ivan O. Rosas, Masahide Takahashi, Naftali Kaminski, Yoshinori Hasegawa

Please cite this article as: Nakahara Y, Hashimoto N, Sakamoto K, *et al*. Fibroblasts positive for meflin have anti-fibrotic property in pulmonary fibrosis. *Eur Respir J* 2021; in press (https://doi.org/10.1183/13993003.03397-2020).

Fibroblasts positive for meflin have anti-fibrotic property in pulmonary fibrosis

Yoshio Nakahara,[a*] Naozumi Hashimoto,[a*#] Koji Sakamoto,[a*] Atsushi Enomoto,[b] Taylor S. Adams,[c] Toyoharu Yokoi,[d] Norihito Omote,[a,c] Sergio Poli,[e] Akira Ando,[a] Keiko Wakahara,[a] Atsushi Suzuki,[a] Masahide Inoue,[a] Akitoshi Hara,[b,f] Yasuyuki Mizutani,[b,g] Kazuyoshi Imaizumi,[h] Tsutomu Kawabe,[i] Ivan O. Rosas,[j] Masahide Takahashi,[b] Naftali Kaminski,[c] Yoshinori Hasegawa[k]

a Department of Respiratory Medicine, Nagoya University Graduate School of Medicine, Nagoya, Japan

b Department of Pathology, Nagoya University Graduate School of Medicine, Nagoya, Japan

c Section of Pulmonary, Critical Care and Sleep Medicine, Yale School of Medicine, New Haven, CT, United States

d Department of Pathology, Tsushima City Hospital, Japan

e Department of Medicine, Mount Sinai Medical Center, Miami Beach, FL, USA

f Department of Cardiology, Nagoya University Graduate School of Medicine, Nagoya, Japan

g Department of Gastroenterology, Nagoya University Graduate School of Medicine, Nagoya, Japan

h Department of Respiratory Medicine and Allergy, Fujita Health University, Toyoake, Japan

i Department of Pathophysiological Laboratory Sciences, Nagoya University Graduate School of Medicine, Nagoya, Japan

j Department of Medicine, Section of Pulmonary, Critical Care and Sleep Medicine, Baylor College of Medicine, Houston, TX, USA

k National Hospital Organization Nagoya Medical Center, Nagoya, Japan

*These authors contributed equally to this work.

#Correspondence and requests for reprint should be addressed to:

Naozumi Hashimoto MD, Department of Respiratory Medicine, Nagoya University Graduate School of Medicine, 65 Tsurumai-cho, Showa-ku, Nagoya 466-8550 Japan;

Tel:+81527442167; Fax:+81527442176; e-mail: hashinao@med.nagoya-u.ac.jp

Disclosure Statement:

N.H. received a research grant from Boehringer Ingelheim, outside the submitted work. T.S.A, S.P, I.O.R., N.K. are inventors on a provisional patent application (62/849,644) that covers methods related to IPF associated cell subsets. N.K. served as a consultant to Biogen Idec, Boehringer Ingelheim, Third Rock, Pliant, Samumed, NuMedii, Indaloo, Theravance, LifeMax, Three Lake Partners, Optikira over the last 3 years and received non-financial support from MiRagen.

Abstract

The prognosis of elderly individuals with idiopathic pulmonary fibrosis (IPF) remains poor. Fibroblastic foci, in which aggregates of proliferating fibroblasts and myofibroblasts are involved, are the pathological hallmark lesions in IPF to represent focal areas of active fibrogenesis. Fibroblast heterogeneity in fibrotic lesions hampers the discovery of the pathogenesis of pulmonary fibrosis. Therefore, to determine of the pathogenesis of IPF, identification of functional fibroblasts is warranted. This study was aimed to determine the role of fibroblasts positive for meflin, identified as a potential marker for mesenchymal stromal cells, during the development of pulmonary fibrosis. We characterized meflin-positive cells in a single cell atlas established by single-cell RNA sequencing (scRNA-seq)-based profiling of 243,472 cells from 32 IPF lungs and 29 normal lung samples. scRNA-seq combined with in situ RNA hybridization identified proliferating fibroblasts positive for meflin in fibroblastic foci, not dense fibrosis, of fibrotic lungs in IPF patients. We determined the role of fibroblasts positive for meflin using bleomycin (BLM)-induced pulmonary fibrosis. A BLM-induced lung fibrosis model for meflin-deficient mice showed that fibroblasts positive for meflin had anti-fibrotic property to prevent pulmonary fibrosis. Although transforming growth factor-β-induced fibrogenesis and cell senescence with senescence-associated secretory

phenotype were exacerbated in fibroblasts via the repression or lack of meflin, these were inhibited in meflin-deficient fibroblasts with meflin reconstitution. These findings provide evidence to show the biological importance of meflin expression on fibroblasts and myofibroblasts in the active fibrotic region of pulmonary fibrosis.

Key words: pulmonary fibrosis, fibroblasts, scRNA-seq, senescence, TGF-β

Introduction

Although clinical advances have been made in pharmacotherapeutic approaches to idiopathic pulmonary fibrosis (IPF) [1], the prognosis of elderly individuals with IPF remains poor with a 5-year survival rate worse than several types of cancer [2]. Although the pathogenesis of IPF remains unclear, some studies on pulmonary fibrosis suggest the potential role of ageing-related responses such as cell senescence in fibroblasts and epithelial cells [3, 4]. The pathological hallmark lesions in IPF comprise fibroblastic foci in fibrotic lesions that may progress to dense fibrosis [5, 6]. Fibroblastic foci have been assumed to represent focal areas of active fibrogenesis, in which aggregates of proliferating fibroblasts and myofibroblasts are involved [7]. sAs fibroblasts isolated from IPF lungs have heterogenous phenotypes and properties different from those of normal lung fibroblasts [8, 9], their diversity makes it difficult to understand the pathogenesis of pulmonary fibrosis [10-14]. Therefore, to determine of the pathogenesis of IPF, identification of functional fibroblasts is warranted.

The advent of single-cell RNA sequencing (scRNA-seq), which enables us to detect well-known or new cell populations without any reliable surface markers [15], has recently identified a new cell type “ionocyte” in the conducting airway epithelium [16, 17]. Although scRNA-seq technologies have successfully defined heterogeneity within

cell populations in fibrotic lungs during the development of pulmonary fibrosis [18-21], they have not fully identified a novel and functional population of fibroblasts with a fibrogenic or anti-fibrogenic phenotype from the fibrotic lungs of IPF patients.

Although meflin-also known as immunoglobulin superfamily containing leucine-rich repeat (ISLR)-has recently been identified as a potential marker for mesenchymal stromal cells (MSC) such as fibroblasts and pericytes [22], the characterization of fibroblasts positive for meflin has not been fully determined in normal or fibrotic lungs. Whether fibroblasts positive for meflin play a critical role during development of pulmonary fibrosis also remains unknown.

The aim of this study was to determine the role of fibroblasts positive for meflin during the development of pulmonary fibrosis.

Results

Bulk and single cell transcriptome profiling for characterization of meflin-expressing cells in normal and IPF lungs

In our microarray dataset previously published, we found that the expression of ISLR mRNA, which encodes meflin protein, was significantly increased in lung homogenate from IPF lungs compared with control lungs in the dataset from Lung Genomics Research Consortium (LGRC) (Gene Expression Omnibus Series [GSE] accession number: 47460) (Figure 1A). To explore the expression profile of ISLR within lung cells of various lineages, we analyzed single-cell transcriptomes of 243,472 cells from 29 normal lung samples and 32 IPF lungs. The analysis with Uniform Manifold Approximation and Projection (UMAP) showed 38 different clusters of cells. Visualization of expression levels with classical markers of cell lineage including immune (PTPRC), epithelial (EPCAM), vascular (CDH5), and stromal (PTGFRB) cell types validated that each cluster has distinct gene expression profiles (Figure 1B and Figure S1A). We roughly stratified the identified clusters into 6 groups according to the observed expression of these classical lineage markers (Figure 1B). In this dataset, the expression of ISLR appeared to be abundant and almost restricted in the PDGFRB+/EPCAM-/CDH5-/PTPRC- group (hereafter PDGFRB+ group) (Figure 1C,

1D, Figure S1B-S1E, and Table S1), which is assumed to include fibroblasts and myofibroblasts by expression of distinct markers, further supported by visualization of positive expression for ACTA2, COL1A1, and COL3A1 (Figure 1C). When we investigated the PDGFRB+ group, we further identified two subgroups (Figure 1E). One subgroup consists of cells from both normal lungs and IPF lungs with scarce expression in ACTA2, the other consists largely of IPF derived cells and frequently positive for ACTA2 expression (Figure 1E). ISLR-positive cells were observed in both subgroups (Figure 1E). Analysis of ISLR expression profiles in single cell resolution using a user-friendly web database [IPF Cell Atlas (http://ipfcellatlas.com/)], validated its distinct expression in stromal cell lineage (Figure S2).

To estimate the function of ISLR-positive stromal cells in normal and disease lung states, we characterized the profiles of genes coordinately expressed with ISLR. We found a set of genes with significant positive correlations with ISLR levels in the PDGFRB+ population (Figure S1F), which included typical fibrosis markers such as COL1A1 (Spearman's rho = 0.312, FDR (false discovery rate) p-value = 4.726e-118), COL3A1 (rho = 0.286, FDR p-value = 1.35E-98), POSTN (rho =0.220, FDR p-value = 3.056E-57), and FN1 (rho = 0.1792, FDR p-value = 1.084E-37). We further stratified cells by lung condition (control lungs or IPF lungs) and conducted gene enrichment

analysis of the top 400 genes with positively correlated ISLR expression (Figure S1G) using GeneGo Metacore software. Process networks such as “cell adhesion” and “proteolysis” were enriched by ISLR-correlated genes in PDGFRB+ cells from both normal and IPF lungs, suggesting their shared functions of ISLR+ stromal cells in normal and disease settings. Meanwhile distinct process networks were also highlighted between normal and IPF fibroblasts. For example, ISLR correlated genes were more enriched in the “proteolysis” process in control lung fibroblasts, while in IPF fibroblasts, processes relevant to “cytoskeleton” processes were enriched (Figure S1G).

Taken together, the above results suggest that ISLR expression is restricted in a cluster of stromal cell lineage in human lungs and is often co-expressed with fibrotic genes such as ACTA2, COL1A1, and COL3A1 (Figure 1C). ISLR-positive cells with ACTA2+ appear increased, particularly in cases of IPF. Gene enrichment analysis of coordinately expressed genes with ISLR implies the functional characteristics of ISLR+ cells, with highlighted cellular processes such as matrix remodeling and cell-matrix interaction.

ISLR expression in lung tissues from healthy subjects and patients with idiopathic pulmonary fibrosis

We determined localization of meflin in lung tissues from 5 subjects with normal lungs (the control group) and 10 patients with pathologically diagnosed IPF (the IPF group) among subjects enrolled in the CHILDREN study. Patient characteristics are shown in Table S2. The levels of ISLR mRNA expression were significantly higher in lung homogenates from the IPF group than in those from the control group (Figure 2A). The IPF group also showed significant increases in COL1A1, ACTA2, and FN1 mRNA expressions, compared with the control group (Figures S3A-S3C). The levels of meflin protein and ISLR mRNA expression were significantly higher in lung fibroblasts derived from the IPF group than in those from the control group (Figure 2B and Figure S3D). Dual ISH for ISLR (meflin) and ACTA2 (α-SMA) was performed (Figures 2C-2L and Figure S4-S6). A previous ISH study suggests that the expression of ISLR is localized in subendothelial or perivascular resident fibroblasts in the bone marrow, adipose tissue, and other organs [22]. ISLR expression was not detected in epithelial, endothelial or alveolar macrophages in normal lungs (Figures 2C and 2D and Figure S3E). Although ISLR-positive fibroblasts were sporadically distributed and scattered in

the perivascular region (shown by a solid line in Figure S3E and Figure 2C) or periepithelial region (shown as a dashed line in Figure S3E and Figure 2D), these cells appeared not to be positive for ACTA2 (Figures 2C and 2D). The lung specimens from 10 patients with IPF were also evaluated by dual ISH for ISLR and ACTA2 (Figures 2E-2L, and Figures S4-S6). The ISH study demonstrated increasing numbers of ISLR-positive fibroblasts were observed in the lesions of fibroblastic foci (shown as solid line in Figures 2E; 2F-2I). Meanwhile, most fibroblasts in the lesions of dense fibrosis (shown by a dashed line in Figures 2E; 2F, and 2J-2L) were myofibroblasts with ACTA2 mRNA expression and only a few ISLR-positive fibroblasts were scattered. When double staining for ISLR and E-cadherin was performed in fibrotic lung tissues, ISLR mRNA expression was not observed in the cells positive for E-cadherin (Figures S3F-S3I). The proportion of ISLR and/or ACTA2-positive fibroblasts were manually quantified in the lesions of fibroblastic foci and dense fibrosis among 10 patients with IPF (Figures 2M-2P). The ISH analysis demonstrated that more than 70% of fibroblasts were positive for ISLR in the lesions of fibroblastic foci, about 50% of which were negative for ACTA2 (Figures 2M and 2N). In dense fibrotic lesions, more than 70% of fibroblasts were ACTA2-positive myofibroblasts; more than 95% of myofibroblasts were negative for ISLR (Figures 2O and 2P).

Anti-fibrotic effect of meflin-positive fibroblasts in an in vivo BLM-induced lung fibrosis model

To evaluate the longitudinal expression of meflin during development of lung fibrosis, BLM-induced lung fibrosis was established in C57BL/6J (WT) mice [10, 11, 23]. Western blotting showed that meflin protein expression increased in a time-dependent manner in BLM, not saline,-treated lungs, followed by *de novo* fibronectin protein expression (Figure 3A and 3B). Real-time PCR showed that the endogenous Islr transcripts were significantly induced in the fibrotic phase during development of pulmonary fibrosis, accompanied by the increasing expressions of fibrogenic variables (Figure 3C and Figures S7A-7F). Next, we determined whether soluble meflin could be detected in bronchoalvaolar lavage (BAL) supernatants. Western blotting showed that there was a significant increase in *de novo* soluble meflin expression were observed in BAL supernatants from BLM-treated lungs, compared with those from saline-treated lungs (Figure 3D). The ISH study for Islr showed that Islr-positive fibroblasts were sporadically distributed and scattered in perivascular or periepithelial regions of the normal mouse lungs, while increasing numbers of Islr-positive cells were observed in the fibrotic lesions on BLM day 14 (Figures 3E-3H and Figures S7G-S7N). To evaluate

the role of meflin expression during development of pulmonary fibrosis, the BLM-induced lung fibrosis model was applied to meflin-deficient mice (meflin KO mice). Lungs from BLM-treated KO mice exhibited more severe pulmonary fibrosis, compared with those from BLM-treated MT mice (Figure 3I). Western blotting and a Sircol collagen assay were performed using lung homogenates from BLM-treated and saline-treated groups day 14 (Figures 3J-3N). Although the saline KO group did not show an increase in fibronectin and α-SMA protein expressions, collagen content, or smad2 activation compared to the saline WT group, the expressions of fibronectin and α-SMA protein, collagen content, and smad2 activation were significantly higher in the BLM-KO group than in the BLM-WT group (Figures 3J-3N). Real-time PCR showed that *de novo* expression of fibrogenic variables including Fn1, Acta2, Col1A1, Tgfb1, and the related mediators, were significantly induced in the BLM KO mice, compared with those in the BLM WT mice (Figure 3O-3R and Figures S7O-S7Z). Taken together, these data clearly suggest a protective role of meflin via anti-fibrotic effects against the development of BLM-induced lung fibrosis *in vivo*.

Anti-fibrotic roles of meflin in primary lung fibroblasts ex vivo against TGF-β-induced fibrogenesis

Our survey of different cell types suggested that meflin was detected in lung fibroblasts, but not in other cells including epithelial, endothelial, and peripheral blood mononuclear cells (Figure S3J and S3K), compatible with a previous study [22]. When naïve primary lung fibroblasts were isolated from WT mice (WT fibroblasts) and meflin KO mice (KO fibroblasts), both cells showed mostly typical spindle-shaped fibroblast morphology (data not shown). The effects of meflin on TGF-β-induced phenotypes in fibroblasts were evaluated by Western blotting, Sircol collagen assay, and realtime PCR (Figures 4A-4E, Figure S8A-S8F, and Figure S8H-S8J). Although primary WT fibroblasts showed meflin protein expression, TGF-β stimulation for 48hours led to more than a 80% decrease in meflin expression in the cells (Figures 4A, 4B, and Figure S8A). The data showed that when no TGF-β was added, KO fibroblasts did not show *de novo* induction of fibronectin, α-SMA, and collagen with smad activation, as compared with WT fibroblasts (Figures 4A, 4C-4E, and Figure S8B-S8F). When these KO fibroblasts were treated with TGF-β, significant increases in fibronectin, α-SMA, and collagen expression with smad activation were observed, compared with that in the WT

fibroblasts (Figures 4A, 4C-4E, and Figure S8B-S8F). To evaluate the effect of meflin on the ability of proliferation in fibroblasts, a WST-1 assay and cell count was performed (Figure 4F and Figure S8G). Both WT fibroblasts and KO fibroblasts showed similar proliferation ability when no TGF-β was added. Although WT fibroblasts treated with TGF-β had slight repression of proliferation compared to the fibroblasts without TGF-β, TGF-β-treated KO fibroblasts remarkably showed no or little proliferation, reminiscent of cell senescence [4, 22, 24]. To evaluate senescence-state cells, SA-βgal staining was performed for these fibroblasts (Figure 4G). Meflin KO fibroblasts treated with TGF-β included a significantly larger number of SA-βgal positive cells when compared to TGF-β-treated WT fibroblasts. Real-time PCR was also performed for relatively reliable cell senescence markers and a senescence-associated secretory phenotype (SASP) such as p16INK4a, p19ARF, Il1b, Il6, and Tgfb1 expressions [4, 24-26]. TGF-β-stimulated KO fibroblasts had significantly increased the expression levels (Figures 4H-4K and Figure S8H-S8J). Furthermore, TGF-β-stimulated KO fibroblasts strikingly showed increased induction of autocrine Tgfb1 transcript, compared with TGF-β-stimulated WT fibroblasts (Figure 4L) [4, 24, 27]. Thus, the repression of or lack of meflin in fibroblasts led to TGF-β-induced aberrant fibrogenesis and senescence with the SASP. To determine

whether meflin expression in fibroblasts is essential for anti-fibrotic effects against TGF-β-induced fibrogenesis and cell senescence, a model of meflin reconstitution was established in KO fibroblasts using lentivirus expressing meflin. The effects of meflin on TGF-β-induced ECM production and α-SMA expression in fibroblasts were evaluated by Western blotting, Sircol collagen assay, and realtime PCR (Figures 4M-4Q and Figure S8K-S8P). Lenti virus-mediated transduction of meflin gene led to the steady expression levels of meflin protein in KO fibroblasts (Figures 4M, 4N and Figure S8K). Meflin reconstitution successfully repressed *de novo* fibronectin, α-SMA, and collagen expressions with smad activation induced by TGF-β (Figures 4O-4Q and Figure S8L-S8P). The effect of meflin reconstitution on TGF-β-induced senescence with SASP was also evaluated. Repression of cell proliferation induced by TGF-β was significantly restored in the meflin-transduced KO fibroblasts, compared with the control transcript-transduced KO fibroblasts (Figure 4R and Figure S8Q). The significantly decreased numbers of SA-βgal-positive cells were also observed in KO fibroblasts with meflin compared to the cells with control (Figure 4S). These repressive effects of meflin reconstitution against cell senescence were accompanied by the inhibition of the related transcripts expressions (Figures 4T-4X and Figure S8R-S8T). When the anti-fibrotic effect of meflin expression was evaluated in normal human lung

fibroblasts (NHLF) using lentivirus expressing meflin, the meflin induction led to the repression of *de novo* fibronectin, α-SMA, and collagen expressions with smad activation induced by TGF-β (Figures 5A-5J). To determine the effect of paracrine meflin on epithelial cells, TGF-β-stimulated lung epithelial cells (MLE-12 cells) were treated with culture medium including soluble meflin (Figure 5K). Although soluble meflin in culture medium repressed TGF-β-induced fibronectin expression in fibroblasts (Figures 5L and 5M), it did not lead to inhibition of the induction of fibronectin expression or restore repression of E-cadherin expression in TGF-β-stimulated MLE-12 cells (Figures 5O-5S).

Discussion

Fibroblasts are central to the progression of lung fibrosis as represented by excessive production of ECM and aberrant tissue contractility [28, 29]. Our unbiased analysis of scRNA-seq data was performed on a larger cohort including 32 IPF patients and 29 control subjects, compared with the previous studies [21, 30]. Assessment of the scRNA-seq data from a total of more than 24,000 lung cells successfully revealed UMAP-based clustering into 6 distinct groups. In our analysis, the cells with ISLR gene expression were substantially classified in the PDGFRB+ group involving fibroblasts and myofibroblasts, while there was nil or little expression of that in other lung cells. In our dual ISH study for ISLR and ACTA2 in human normal lungs, very few fibroblasts were positive for ISLR and did not appear to express ACTA2 transcripts, compatible with scRNA-seq analysis. Thus, we identified that ISLR gene-encoding meflin is substantially expressed in fibroblasts of normal lungs as a rare cell population through combined analysis of scRNA-seq and ISH studies.

Fibroblastic foci, active “new” areas of fibrosis, are pathologically found at the interface between normal parenchyma and scarred “old” areas of fibrosis with dense collagen deposition and smooth muscle proliferation [5, 6, 31, 32]. Our data suggest that fibroblasts/myofibroblasts positive for meflin might be closely associated with the

pathogenesis for development of fibroblastic foci, active “new” areas of fibrosis, in IPF. While there is no completely satisfactory animal model of human IPF, the BLM-induced model is relatively well characterized and does exhibit certain features also found in human disease [18-20]. The numbers of fibroblasts positive for meflin increased in the fibrotic lesions of BLM-induced mouse injured lungs as those observed in fibroblastic foci of IPF lungs. Although recent studies suggested that fibroblasts with meflin expression inhibit not only tumor progression as cancer-associated fibroblasts but also the development of cardiac fibrosis as cardiac fibroblasts [33, 34], there has been little understanding or characterization of fibroblasts positive for meflin in normal and fibrotic lungs [22]. The BLM-induced meflin KO mice model reveals that meflin-positive fibroblasts have anti-fibrotic properties that prevent exacerbation of local microinjuries and consequently fibrosis. These findings might provide the basis to identify the underlying mechanisms by which meflin-expressing fibroblasts emerge in fibrotic foci, not dense fibrosis, of IPF lungs. In this study, it was hard to determine whether meflin expression might be associated with clinical parameters including the fibrotic findings evaluated by thin-section computed tomography (TSCT), possibly due to the relatively small numbers of patients (10 IPF patients). Although it remains difficult to distinguish fibrotic foci from dense fibrosis in IPF lungs using TSCT scan

[35-37], our study demonstrated that soluble meflin could be detected in BAL supernatants in parallel with fibrotic activity of BLM-induced lung fibrosis. It encourages us to estimate soluble meflin in BAL supernatants as a biomarker of disease activity in IPF lungs. Although aberrant epithelial-fibroblast communication with activated TGF-β signaling might be assumed to be the pathogenesis of pulmonary fibrosis [3, 32], soluble meflin did not appear to inhibit TGF-β-induced fibrogenesis in epithelial cells *in vitro*.

Cellular senescence has been recently implicated in the pathogenesis of fibrosis [4, 24]. Although senescent fibroblasts were shown to exacerbate fibrogenesis through secretion of the SASP factors [4, 25, 26, 38], the secretome of senescent epithelial cells might not activate a fibrogenic response in fibroblasts [4]. Moreover, recent studies showed that TGF-β stimulation might induce cellular senescence [24, 39]. Our data demonstrate that fibroblasts positive for meflin negatively regulates TGF-β-induced cellular senescence and fibrogenesis. Although TGF-β repressed meflin expression in primary WT fibroblasts, the lack of or repression of meflin in fibroblasts yielded TGF-β-induced cellular senescence [25, 26]. The induction of autocrine TGF-β transcript expression by paracrine TGF-β1 stimulation was augmented in primary meflin KO fibroblasts. Consequently, ECM productions and increased α-SMA expression were accelerated in

meflin KO fibroblasts via paracrine and autocrine TGF-β stimulation [4, 24-26, 38]. The exact mechanism by which meflin regulates TGF-β-induced cell senescence and fibrogenesis has not been fully determined [22, 40]. Nevertheless, the reconstitution of meflin in primary KO fibroblasts blunted TGF-β-induced cell senescence with SASP, followed by the repression of TGF-β-induced fibrogenesis. Furthermore, the induction of meflin into human lung fibroblasts repressed *de novo* fibronectin, α-SMA, and collagen expressions with smad activation induced by TGF-β. Our findings provide evidence with which to determine the biological importance of meflin expression on TGF-β-induced cell senescence and fibrogenesis in fibroblasts and myofibroblasts. Furthermore, the targeting of TGF-β signaling was demonstrated to reduce the development of senescence and improved survival in a mouse model of acute liver injury and failure [24]. Thus, further investigation is warranted, to explore how to approach the enhancement of meflin expression on fibroblasts and myofibroblasts in the active fibrotic region of pulmonary fibrosis.

In summary, three remarkable findings are highlighted (Figure 6). A new therapeutic strategy for pulmonary fibrosis might be warranted according to the data showing repressive effect of meflin reconstitution into fibroblasts against TGF-β-induced fibrogenesis and cell senescence.

Material and methods

A detailed description of the methods is provided in the supplementary material.

Analysis of microarray data of human samples

We analyzed data set GSE47460 -GPL14550 for ISLR transcript levels in normal lungs and lungs of IPF patients. Log2-transformed normalized expression values for ISLR gene in 122 IPF lungs and 91 control lungs were retrieved using GEO2R and visualized using GraphPad Prism Version 7 (GraphPad Software, San Diego, CA).

Sample preparation for single cell sequencing

IPF lungs were obtained from patients undergoing transplants while healthy lungs comprised rejected donor lung organs that underwent lung transplantation at the Brigham and Women's Hospital or donor organs provided by the National Disease Research Interchange (NDRI). The study protocol was approved by the Partners Healthcare Institutional Board Review (IRB Protocol # 2011P002419).

Sample preparation in the CHILDREN registry

Human lung tissue samples from 10 patients with IPF and 5 subjects with normal lungs were obtained via surgical lung biopsy or remnants of lung resection at Nagoya

University Hospital. All study subjects were enrolled in the CHILDREN registry (the CHronic Interstitial Lung Disease REgistry of Nagoya University), which were approved by the Nagoya University Ethics Committee (Approval date: December, 20, 2018; Approval#:2017-0169-3).

Mouse fibrosis model

Pulmonary fibrosis was induced by endotracheal BLM injection as previously described [10, 11]. All animal studies were reviewed and approved by the University Committee on Use and Care of Animals at Nagoya University Graduate School of Medicine (Approval date: March 22, 2019; Approval#: 31333).

Statistical analysis

Data were presented as median ± range when specified. Comparison of two groups was performed using unpaired Student's t-test (parametric) or Mann- Whitney U-test (non-parametric). For multiple comparison, we used a repeated measures ANOVA with post-hoc Bonferroni's test or a one-way ANOVA with post-hoc Tukey's test to determine the significance. Kaplan-Meier survival estimation with a log-rank test was performed to compare the animal survival rate between treatment groups. All statistical

analyses were performed using SPSS statistical software (IBM Corp, Chicago, IL). A value < 0.05 was considered statistically significant.

Author contributions

Y.N., N.H., and K.S. developed the concept and design of the study.

Y.N., N.H., K.S., N.O., A.A., K.W., A.S., M.I., A.H. and Y.M., acquired data.

Y.N., N.H., K.S., and T.S.A., provided analyses.

Y.N., N.H., and K.S., were involved in interpretation of data.

T.Y. performed pathological assessment.

A.E., T.S.A., SP, I.O.R., and N.K. provided essential material.

Y.N. and N.H. wrote the manuscript.

M.T., K.I., T.K., I.O.R, N.K., and Y.H. contributed to scientific discussion.

All authors reviewed and approved the manuscript.

Acknowledgments

We are indebted to all patients and control subjects who participated in this study. This work was supported by Grant-in-Aid for Young Scientists (B) (18K15948) to K.S., AMED-CREST (Japan Agency for Medical Research and Development, Core Research for Evolutional Science and Technology; 20gm1210009s0102 and 20gm0810007h0105)

to A.E. and M.T., Grant-in-Aid for challenging Exploratory Research (20K21599) to N.H., CREST (Core Research for Evolutional Science and Technology; JPMJCR17H3) to N.H, and the 24th Promotion Fund of the Annual Meeting of the Medical Society of Japan Commemorative Medicine to N.H. This work was also supported by NIH grants R01HL127349, U01HL145567, U01HL122626, and U54HG008540 to N.K, NHLBI P01 HL114501 and support from the Pulmonary Fibrosis Fund to I.O.R., an unrestricted gift from Three Lake Partners to I.O.R and N.K.

References

1. Lederer DJ, Martinez FJ. Idiopathic Pulmonary Fibrosis. N Engl J Med 2018; 378(19):1811-1823.

2. du Bois RM. An earlier and more confident diagnosis of idiopathic pulmonary fibrosis. Eur Respir Rev 2012; 21(124):141-146.

3. Mora AL, Rojas M, Pardo A *et al*. Emerging therapies for idiopathic pulmonary fibrosis, a progressive age-related disease. Nat Rev Drug Discov 2017; 16(11):755-772.

4. Schafer MJ, White TA, Iijima K *et al*. Cellular senescence mediates fibrotic pulmonary disease. Nat Commun 2017; 8:14532.

5. King TE, Jr., Schwarz MI, Brown K *et al*. Idiopathic pulmonary fibrosis: relationship between histopathologic features and mortality. Am J Respir Crit Care Med 2001; 164(6):1025-1032.

6. Nicholson AG, Fulford LG, Colby TV *et al*. The relationship between individual histologic features and disease progression in idiopathic pulmonary fibrosis. Am J Respir Crit Care Med 2002; 166(2):173-177.

7. Katzenstein AL, Myers JL. Idiopathic pulmonary fibrosis: clinical relevance of pathologic classification. Am J Respir Crit Care Med 1998; 157(4 Pt 1):1301-1315.

8. Thannickal VJ, Toews GB, White ES *et al*. Mechanisms of pulmonary fibrosis. Annu Rev Med 2004; 55:395-417.

9. Wynn TA. Integrating mechanisms of pulmonary fibrosis. J Exp Med 2011; 208(7):1339-1350.

10. Hashimoto N, Jin H, Liu T *et al*. Bone marrow-derived progenitor cells in pulmonary fibrosis. J Clin Invest 2004; 113(2):243-252.

11. Hashimoto N, Phan SH, Imaizumi K *et al*. Endothelial-mesenchymal transition in bleomycin-induced pulmonary fibrosis. Am J Respir Cell Mol Biol 2010; 43(2):161-172.

12. Rock JR, Barkauskas CE, Cronce MJ *et al*. Multiple stromal populations contribute to pulmonary fibrosis without evidence for epithelial to mesenchymal transition. Proc Natl Acad Sci U S A 2011; 108(52):E1475-1483.

13. Ubil E, Duan J, Pillai IC *et al*. Mesenchymal-endothelial transition contributes to cardiac neovascularization. Nature 2014; 514(7524):585-590.

14. Xie T, Liang J, Liu N *et al*. Transcription factor TBX4 regulates myofibroblast accumulation and lung fibrosis. J Clin Invest 2016; 126(8):3063-3079.

15. Grun D, van Oudenaarden A. Design and Analysis of Single-Cell Sequencing Experiments. Cell 2015; 163(4):799-810.

16. Montoro DT, Haber AL, Biton M *et al*. A revised airway epithelial hierarchy includes CFTR-expressing ionocytes. Nature 2018; 560(7718):319-324.

17. Plasschaert LW, Zilionis R, Choo-Wing R *et al*. A single-cell atlas of the airway epithelium reveals the CFTR-rich pulmonary ionocyte. Nature 2018; 560(7718):377-381.

18. Zepp JA, Zacharias WJ, Frank DB *et al*. Distinct Mesenchymal Lineages and Niches Promote Epithelial Self-Renewal and Myofibrogenesis in the Lung. Cell 2017; 170(6):1134-1148 e1110.

19. Xie T, Wang Y, Deng N *et al*. Single-Cell Deconvolution of Fibroblast Heterogeneity in Mouse Pulmonary Fibrosis. Cell Rep 2018; 22(13):3625-3640.

20. Peyser R, MacDonnell S, Gao Y *et al*. Defining the Activated Fibroblast Population in Lung Fibrosis Using Single Cell Sequencing. Am J Respir Cell Mol Biol 2019.

21. Reyfman PA, Walter JM, Joshi N *et al*. Single-Cell Transcriptomic Analysis of Human Lung Provides Insights into the Pathobiology of Pulmonary Fibrosis. Am J Respir Crit Care Med 2019; 199(12):1517-1536.

22. Maeda K, Enomoto A, Hara A *et al*. Identification of Meflin as a Potential Marker for Mesenchymal Stromal Cells. Sci Rep 2016; 6:22288.

23. Sakamoto K, Hashimoto N, Kondoh Y *et al*. Differential modulation of surfactant protein D under acute and persistent hypoxia in acute lung injury. Am J Physiol Lung Cell Mol Physiol 2012; 303(1):L43-53.

24. Bird TG, Muller M, Boulter L *et al*. TGFbeta inhibition restores a regenerative response in acute liver injury by suppressing paracrine senescence. Sci Transl Med 2018; 10(454).

25. Coppe JP, Patil CK, Rodier F *et al*. Senescence-associated secretory phenotypes reveal cell-nonautonomous functions of oncogenic RAS and the p53 tumor suppressor. PLoS Biol 2008; 6(12):2853-2868.

26. Coppe JP, Desprez PY, Krtolica A *et al*. The senescence-associated secretory phenotype: the dark side of tumor suppression. Annu Rev Pathol 2010; 5:99-118.

27. Sheppard D. Pulmonary fibrosis: a cellular overreaction or a failure of communication? J Clin Invest 2001; 107(12):1501-1502.

28. Herrera J, Henke CA, Bitterman PB. Extracellular matrix as a driver of progressive fibrosis. J Clin Invest 2018; 128(1):45-53.

29. Lynch MD, Watt FM. Fibroblast heterogeneity: implications for human disease. J Clin Invest 2018; 128(1):26-35.

30. Xu Y, Mizuno T, Sridharan A *et al*. Single-cell RNA sequencing identifies diverse roles of epithelial cells in idiopathic pulmonary fibrosis. JCI Insight 2016; 1(20):e90558.

31. Smith M, Dalurzo M, Panse P *et al*. Usual interstitial pneumonia-pattern fibrosis in surgical lung biopsies. Clinical, radiological and histopathological clues to aetiology. J Clin Pathol 2013; 66(10):896-903.

32. Richeldi L, Collard HR, Jones MG. Idiopathic pulmonary fibrosis. Lancet 2017; 389(10082):1941-1952.

33. Hara A, Kobayashi H, Asai N *et al*. Roles of the Mesenchymal Stromal/Stem Cell Marker Meflin in Cardiac Tissue Repair and the Development of Diastolic Dysfunction. Circ Res 2019; 125(4):414-430.

34. Mizutani Y, Kobayashi H, Iida T *et al*. Meflin-Positive Cancer-Associated Fibroblasts Inhibit Pancreatic Carcinogenesis. Cancer Res 2020; 79(20):5367-5381.

35. Hashimoto N, Ando A, Iwano S *et al*. Thin-section computed tomography-determined usual interstitial pneumonia pattern affects the decision-making process for resection in newly diagnosed lung cancer patients: a retrospective study. BMC Pulm Med 2018; 18(1):2.

36. Luzina IG, Salcedo MV, Rojas-Pena ML *et al*. Transcriptomic evidence of immune activation in macroscopically normal-appearing and scarred lung tissues in idiopathic pulmonary fibrosis. Cell Immunol 2018; 325:1-13.

37. McDonough JE, Ahangari F, Li Q *et al*. Transcriptional regulatory model of fibrosis progression in the human lung. JCI Insight 2019; 4(22).

38. Alvarez D, Cardenes N, Sellares J *et al*. IPF lung fibroblasts have a senescent phenotype. Am J Physiol Lung Cell Mol Physiol 2017; 313(6):L1164-L1173.

39. Rapisarda V, Borghesan M, Miguela V *et al*. Integrin Beta 3 Regulates Cellular Senescence by Activating the TGF-beta Pathway. Cell Rep 2017; 18(10):2480-2493.

40. Nagasawa A, Kubota R, Imamura Y *et al*. Cloning of the cDNA for a new member of the immunoglobulin superfamily (ISLR) containing leucine-rich repeat (LRR). Genomics 1997; 44(3):273-279.

Figure legends

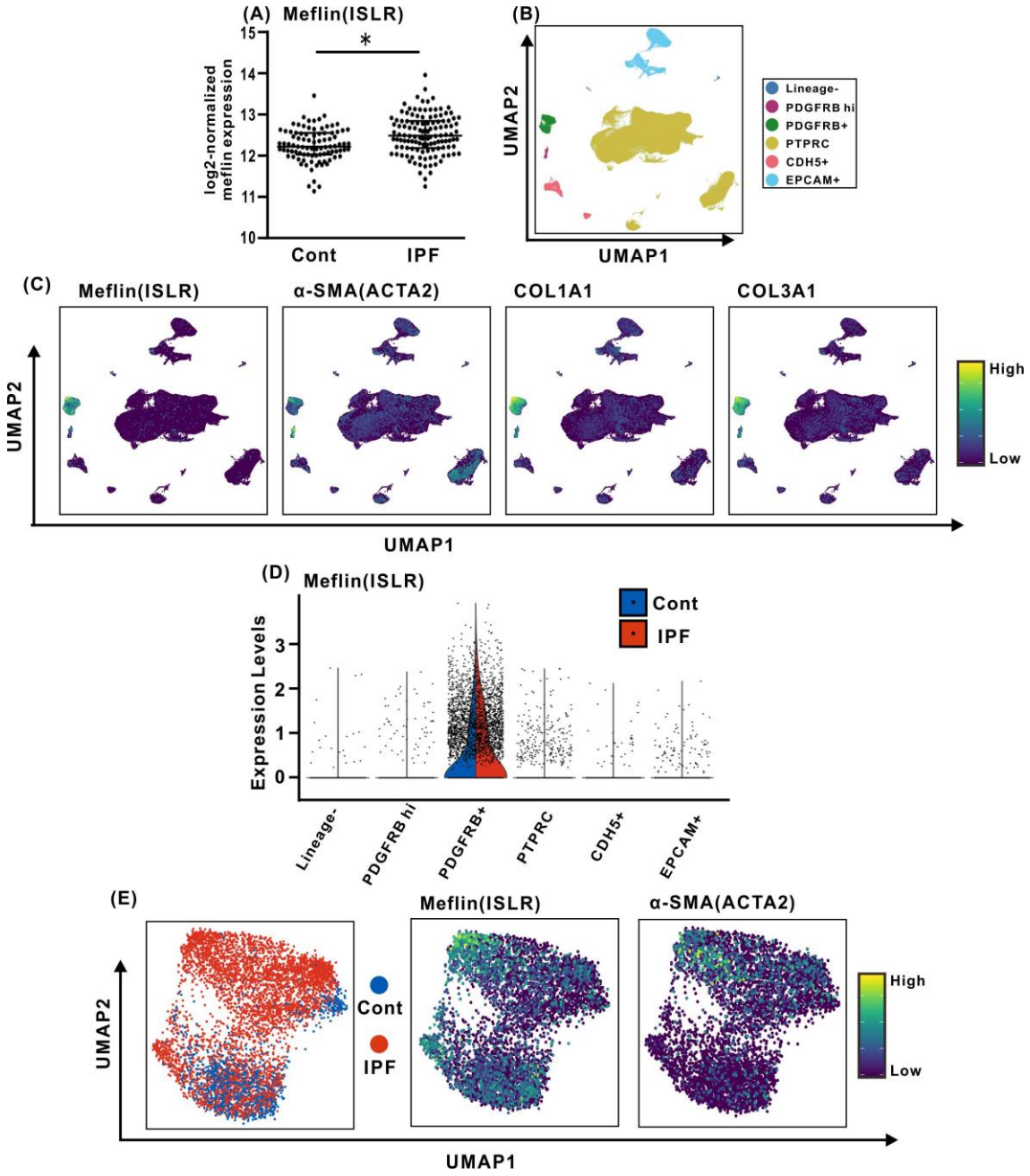

Figure 1. ***Single Cell RNAseq analysis of ISLR expression in human lung scRNAseq data***

(A) Normalized expression of ISLR mRNA in lung homogenates from IPF (n = 122; IPF) and control (n = 91; Cont) lungs. Data were obtained from the published microarray dataset (GSE47460 – GPL14550). * p <0.0001 (Mann–Whitney U-test between two variables). (**B)** The labeling of clusters stratified according to the expression of classical cell markers by UMAP. Classical cell markers for immune (PRPRC), epithelial (EPCAM), endothelial (CDH5), and mesenchymal (PDGFRB) cell populations, respectively. (**C)** Feature plots showing normalized gene expression of ISLR and other genes relevant to lung fibrosis (ACTA2, COL1A1, and COL3A1). (**D)** Violin plots showing expression of ISLR is restricted in PDGFRB+ cluster. (**E)** Distribution of ISLR expression within PDGFRB+ cluster. Left panel indicates the origins of the cells stratified by disease state (control or IPF), middle and left panel indicate the expression levels of ISLR and ACTA2, respectively. Red dashed circles indicate a part of the subgroup positive for ACTA2 with higher ISLR expression.

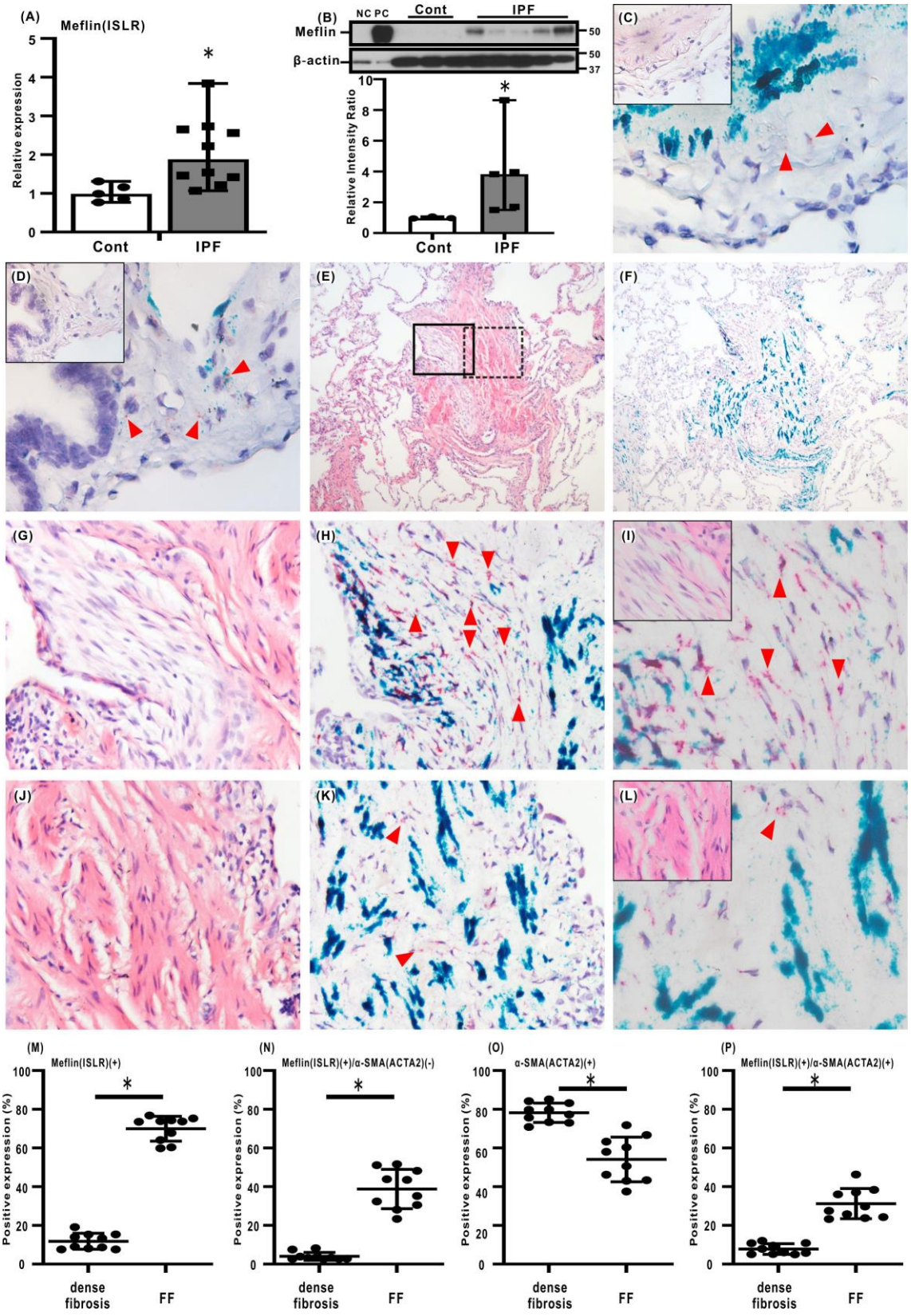
(A)
Meflin(ISLR)
Relative expression
Cont
IPF
(B)
NC PC
Cont
IPF
Meflin
β-actin
50
50
37
Relative Intensity Ratio
Cont
IPF
(C)
(D)
(E)
(F)
(G)
(H)
(I)
(J)
(K)
(L)
(M)
Meflin(ISLR)(+)
Positive expression (%)
dense fibrosis
FF
(N)
Meflin(ISLR)(+)/α-SMA(ACTA2)(-)
(O)
α-SMA(ACTA2)(+)
(P)
Meflin(ISLR)(+)/α-SMA(ACTA2)(+)

Figure 2. ***Meflin expression in lung tissues from healthy subjects and patients with idiopathic pulmonary fibrosis***

(**A**) The expression of ISLR transcripts were evaluated in lung homogenates from IPF (n = 10) and control (n = 5) lungs among subjects enrolled in the CHILDREN study. *P < 0.05 in comparison with control group. (**B**) The meflin protein expressions were evaluated in lung fibroblasts derived from IPF (n = 5) and control (n = 3) lungs among subjects enrolled in the CHILDREN study. *P < 0.05 in comparison with control group. The ISH for ISLR (red) and ACTA2 (green) (**C**) and H-E staining (inset in (**C**)) were shown for the lined box area in (Figure S3E). X400 magnification. The ISH for ISLR (red) and ACTA2 (green) (**D**) and H-E staining (inset in (**D**)) were shown for the dotted box area in (Figure S3E). X400 magnification. H-E staining (**E**) and the ISH for ISLR (red) and ACTA2 (green) (**F**) were performed for representative lung sections from IPF group (case 193). X40 magnification. The lined box area and dotted box area in (**E**) indicate fibrotic foci region and dense fibrosis region, respectively. H-E staining were shown for lined box area (**G**) and dotted box area (**J**), respectively. X200 magnification. The ISH for ISLR (red) and ACTA2 (green) were also shown for lined box area (**H**) and dotted box area (**K**), respectively. X200 magnification. H-E staining (inset in (**I**)) and the ISH for ISLR (red) and

ACTA2 (green) (**I**) were shown for lined box area in (**E**). X400 magnification. H-E staining (inset in (**L**)) and the ISH for ISLR (red) and ACTA2 (green) (**L**) were shown for the dotted box area in (**E**). X400 magnification. The red arrowheads (**H**, **I**, **K**, and **L**) indicate meflin positive cells. The percentage of ISLR and/or ACTA2-positive cells that colocalized with nuclei in fibrotic foci and dense fibrosis were shown in (**M**), (**N**), (**O**), and (**P**). *$P < 0.05$ in comparison with dense fibrosis. (**A**), (**B**) and (**M**)-(**P**): Mann–Whitney U-test.

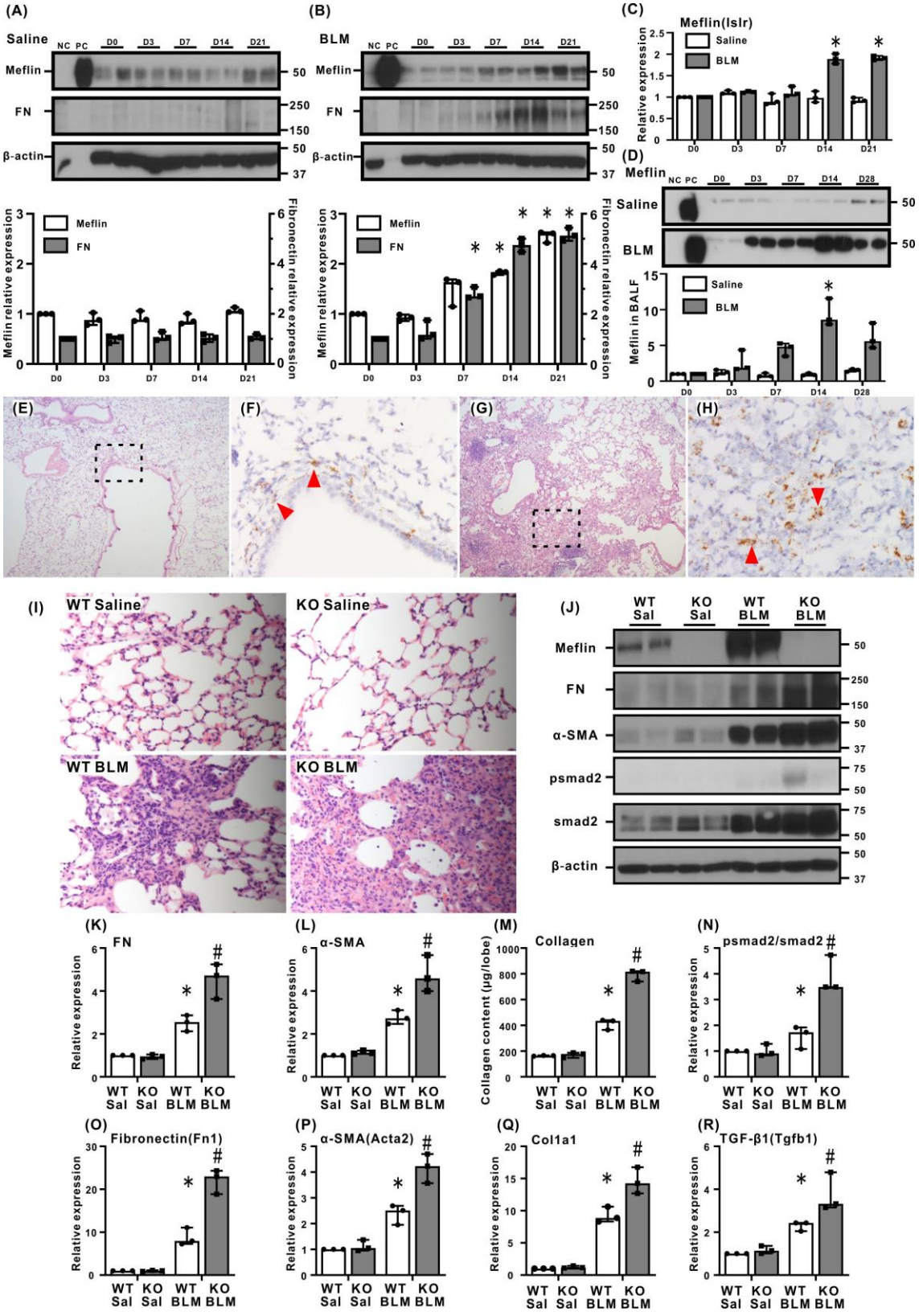
(A)
Saline
NC PC D0 D3 D7 D14 D21
Meflin
FN
β-actin
50
250
150
50
37
(B)
BLM
NC PC D0 D3 D7 D14 D21
Meflin
FN
β-actin
50
250
150
50
37
(C)
Meflin(Islr)
Saline
BLM
Relative expression
D0 D3 D7 D14 D21
(D)
Meflin
NC PC D0 D3 D7 D14 D28
Saline
BLM
50
50
Saline
BLM
Meflin in BALF
D0 D3 D7 D14 D28
Meflin
FN
Meflin relative expression
Fibronectin relative expression
D0 D3 D7 D14 D21
Meflin
FN
Meflin relative expression
Fibronectin relative expression
D0 D3 D7 D14 D21
(E)
(F)
(G)
(H)
(I)
WT Saline
KO Saline
WT BLM
KO BLM
(J)
WT Sal
KO Sal
WT BLM
KO BLM
Meflin
FN
α-SMA
psmad2
smad2
β-actin
50
250
150
50
37
75
50
75
50
50
37
(K)
FN
Relative expression
WT Sal
KO Sal
WT BLM
KO BLM
(L)
α-SMA
Relative expression
(M)
Collagen
Collagen content (μg/lobe)
(N)
psmad2/smad2
Relative expression
(O)
Fibronectin(Fn1)
Relative expression
(P)
α-SMA(Acta2)
Relative expression
(Q)
Col1a1
Relative expression
(R)
TGF-β1(Tgfb1)
Relative expression

Figure 3. ***Anti-fibrotic effect of meflin-positive fibroblasts in an in vivo BLM-induced lung fibrosis model***

Western blot analyses of meflin, fibronectin (FN), β-actin in lung homogenates from saline-treated mice (**A**) and BLM-treated mice (**B**) at the indicated time were performed. A representative blot is shown at upper panel in (**A**) and (**B**). NC: cell lysate of 293FT cells. PC: cell lysate of 293FT cells stably expressing mouse Islr. The intensity of expressions was evaluated and shown after normalization to β-actin expression at lower panel in (**A**) and (**B**). Meflin: white square; FN: gray square. *P < 0.05 in comparison with D0. Realtime PCR analyses for Islr (**C**) were performed for lung homogenates from saline-treated mice and BLM-treated mice collected at the indicate time. *P < 0.05 in comparison with D0. (**D**) Western blot analyses of meflin was performed for bronchoalvaolar lavage (BAL) supernatants (2μg of total protein per per sample) from saline-treated mice and BLM-treated mice at the indicated time. A representative blot is shown in the upper panel in (**D**) (upper panel: saline, lower panel: BLM). The intensity of expressions was evaluated and is shown in the lower panel in (**D**). *P < 0.05 in comparison with D0. Representative lung sections from saline-treated mice (**E** and **F**) and BLM-treated mice (**G** and **H**) were examined by H-E staining (**E** and **G**) and the ISH for Islr (brown) (**F** and **H**). The dotted box areas in

(**E**) and (**G**) indicate periepithelial region and fibrotic region, respectively. The red arrowheads in (**F**) and (**H**) indicate Islr-positive cells. Original magnification: X200. (**I**) The BLM-induced lung fibrosis model was applied to wild (WT) mice and meflin-deficient (KO) mice (WT saline n = 6, KO saline n = 6, WT BLM n = 9, KO BLM n = 9, respectively). Representative histologic sections of lung tissue obtained at day 14 following BLM or saline challenge in WT and KO mice. Original magnification: X200. (**J**) Western blot analyses of meflin, fibronectin (FN), α-SMA, phosphorylated smad2 (psmad2), smad2, and β-actin in lung homogenates from treated mice were performed. A representative blot is shown in (**J**). The intensity of expressions of FN (**K**) and α-SMA (**L**), were evaluated and shown after normalization to β-actin expression. The collagen content (**M**) evaluated by Sircol collagen assay is also shown. (**N**) The ratio of psmad2 to smad2 was presented as the intensity level. Realtime PCR analyses for Fn1 (**O**), Acta2 (**P**), Col1a1 (**Q**), and Tgfb1 (**R**), were performed for lung homogenates from treated mice. *P < 0.05 in comparison with saline-treated WT mice. # P < 0.05 in comparison with BLM-treated WT mice. (**A**-**D**): repeat-measures ANOVA with post-hoc Bonferroni's test. (**I**): Log-rank test. (**K**-**R**): one-way ANOVA with post-hoc Tukey's test. The experiment was repeated three times with similar results.

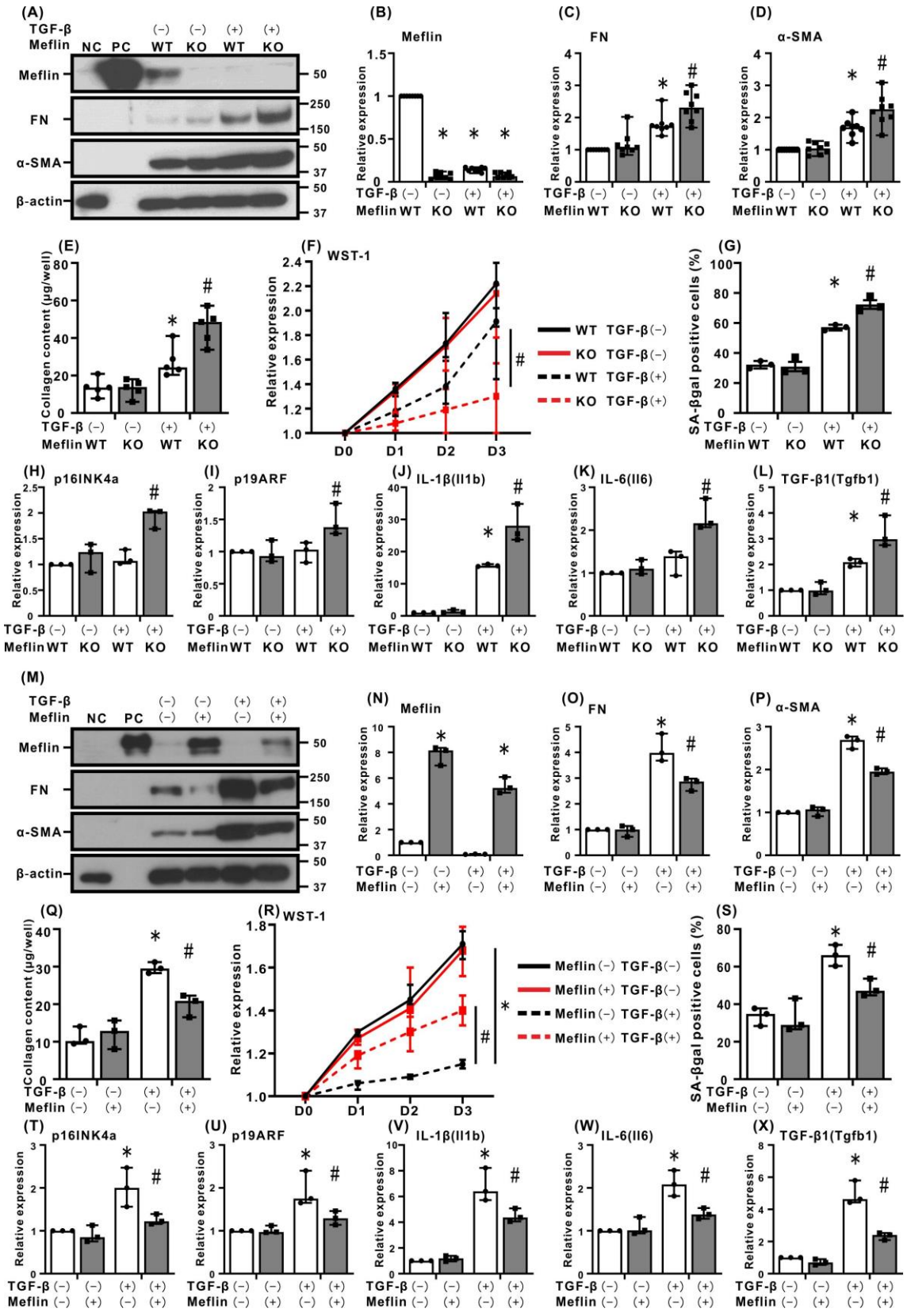
(A)
TGF-β
Meflin
NC PC WT KO WT KO
Meflin
FN
α-SMA
β-actin
(B) Meflin
(C) FN
(D) α-SMA
Relative expression
(E) Collagen content (μg/well)
(F) WST-1
WT TGF-β(−)
KO TGF-β(−)
WT TGF-β(+)
KO TGF-β(+)
D0 D1 D2 D3
(G) SA-βgal positive cells (%)
(H) p16INK4a
(I) p19ARF
(J) IL-1β(Il1b)
(K) IL-6(Il6)
(L) TGF-β1(Tgfb1)
(M)
(N) Meflin
(O) FN
(P) α-SMA
(Q) Collagen content (μg/well)
(R) WST-1
Meflin (−) TGF-β(−)
Meflin (+) TGF-β(−)
Meflin (−) TGF-β(+)
Meflin (+) TGF-β(+)
(S) SA-βgal positive cells (%)
(T) p16INK4a
(U) p19ARF
(V) IL-1β(Il1b)
(W) IL-6(Il6)
(X) TGF-β1(Tgfb1)

Figure 4. ***Anti-fibrotic roles of meflin in primary mouse lung fibroblasts ex vivo against TGF-β-induced fibrogenesis***

Western blot analyses of meflin, fibronectin, β-actin in control or TGF-β-stimulated primary lung WT and KO fibroblasts were performed. A representative blot is shown in (**A**). The intensity of expressions of meflin (**B**), fibronectin (FN) (**C**), α-SMA (**D**), were evaluated and shown after normalization to β-actin expression. The collagen content of cell lysate (**E**) evaluated by Sircol collagen assay is shown. A WST-1 assay was performed for control or TGF-β-stimulated primary lung fibroblasts from WT and KO mice (**F**). The numbers of SA-βgal-positive cells were also evaluated in control or TGF-β-stimulated primary lung fibroblasts from WT and KO mice (**G**). Realtime PCR analyses for p16INK4a (**H**), p19ARF (**I**), Il1b (**J**), Il6 (**K**), and Tgfb1 (**L**), were performed in control or TGF-β-stimulated primary lung fibroblasts from WT and KO mice. *$P < 0.05$ in comparison with control-stimulated fibroblasts from WT mice. # $P < 0.05$ in comparison with TGF-β-stimulated fibroblasts from WT mice. Western blot analyses of meflin, fibronectin, β-actin in control or TGF-β-stimulated primary lung KO fibroblasts, for which control or meflin were reconstituted by using lenti virus, were performed. A representative blot is shown in (**M**). The intensity of expressions of meflin (**N**), FN (**O**), α-SMA (**P**), were evaluated and shown after

normalization to β-actin expression. The collagen content of cell lysate (**Q**) evaluated by Sircol collagen assay is shown. A WST-1 assay was performed for these cells (**R**). The numbers of SA-βgal-positive cells were also evaluated (**S**). Realtime PCR analyses for p16INK4a(**T**), p19ARF (**U**), Il1b (**V**), Il6 (**W**), and TgfbG1 (**X**), were also performed in control or TGF-β-stimulated primary lung fibroblasts from KO mice, for which control or meflin were reconstituted. *P < 0.05 in comparison with control-stimulated KO fibroblasts with control gene induction. # P < 0.05 in comparison with TGF-β-stimulated KO fibroblasts with control gene induction. NC: cell lysate of 293FT cells. PC: cell lysate of 293FT cells stably expressing mouse Islr. (**F** and **R**): repeat-measures ANOVA with post-hoc Bonferroni's test. (**B-E, G-L, N-Q, and S-X**): one-way ANOVA with post-hoc Tukey's test. The experiment was repeated at least three times with similar results.

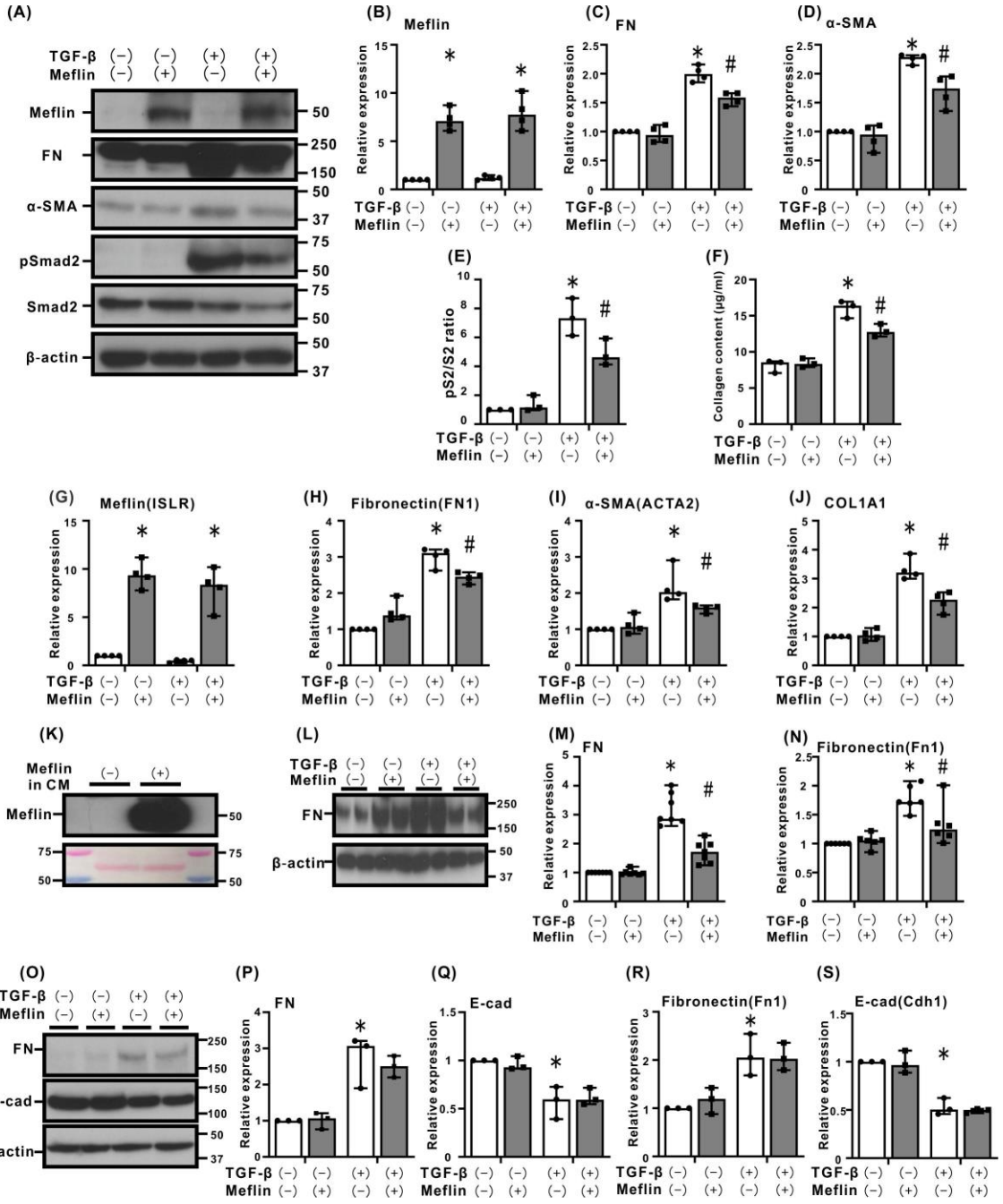
(A)
TGF-β (−) (−) (+) (+)
Meflin (−) (+) (−) (+)
Meflin
FN
α-SMA
pSmad2
Smad2
β-actin
50
250
150
50
37
75
50
75
50
50
37
(B) Meflin
(C) FN
(D) α-SMA
Relative expression
(E) pS2/S2 ratio
(F) Collagen content (μg/ml)
(G) Meflin(ISLR)
(H) Fibronectin(FN1)
(I) α-SMA(ACTA2)
(J) COL1A1
(K)
Meflin in CM
(L)
(M) FN
(N) Fibronectin(Fn1)
(O)
E-cad
(P) FN
(Q) E-cad
(R) Fibronectin(Fn1)
(S) E-cad(Cdh1)

Figure 5. ***Anti-fibrotic effect of meflin in human lung fibroblasts and no anti-fibrotic effect of soluble meflin in epithelial cells against TGF-β-induced fibrogenesis***

Western blot analyses were performed of meflin, fibronectin (FN), α-SMA, phosphorylated smad2 (psmad2), smad2, and β-actin in control or TGF-β-stimulated normal human adult lung fibroblasts (NHLF), for which control or human meflin were reconstituted by using lentivirus. A representative blot is shown in (**A**). The intensity of expressions of meflin (**B**), FN (**C**), and α-SMA (**D**), were evaluated and shown after normalization to β-actin expression. The ratio of psmad2 to smad2 is presented as the intensity level (**E**). The collagen content of conditioned medium collected from reconstituted fibroblasts was evaluated by Sircol collagen assay (**F**). Realtime PCR analyses for ISLR (**G**), FN1 (**H**), ACTA2 (**I**), and COL1A1 (**J**), were performed in control or TGF-β-stimulated NHLF. *$P < 0.05$ in comparison with control-stimulated NHLF with control gene induction. # $P < 0.05$ in comparison with TGF-β-stimulated NHLF with control gene induction. Western blot analysis of meflin was performed for culture medium (CM) (10μg of total protein per sample) from 293FT cells or 293FT cells stably expressing mouse Islr (**K**, upper). Ponceau S staining was also performed for total protein normalization (**K,** lower). A

representative blot is shown in (**K**). (**L**) Western blot analyses of fibronectin (FN) and β-actin were performed in control or TGF-β-stimulated primary lung KO fibroblasts treated with culture medium from 293FT cells or 293FT cells stably expressing mouse Islr. A representative blot is shown. The intensity of expressions of FN (**M**) were evaluated and are shown after normalization to β-actin expression. Realtime PCR analysis for Fn1 (**N**) was also performed for the cells. *P < 0.05 in comparison with control-stimulated KO fibroblasts with control culture medium. # P < 0.05 in comparison with TGF-β-stimulated KO fibroblasts with control culture medium. (**O**) Western blot analyses of fibronectin (FN), E-cadherin (E-cad), and β-actin were performed in control or TGF-β-stimulated mouse epithelial cells (MLE-12 cells) treated with culture medium from 293FT cells or 293FT cells stably expressing mouse Islr. A representative blot is shown. The intensity of expressions of FN (**P**) and E-cad (**Q**) were evaluated and are shown after normalization to β-actin expression. Realtime PCR analyses for Fn1 (**R**) and Cdh1 (**S**) were also performed for the cells. *P < 0.05 in comparison with control-stimulated MLE-12 cells with control culture medium. # P < 0.05 in comparison with TGF-β-stimulated MLE-12 cells with control culture medium. (**B**-**J** and **M**-**S**): a one-way ANOVA with post-hoc Tukey's test. The experiment was repeated at least three times with similar results.

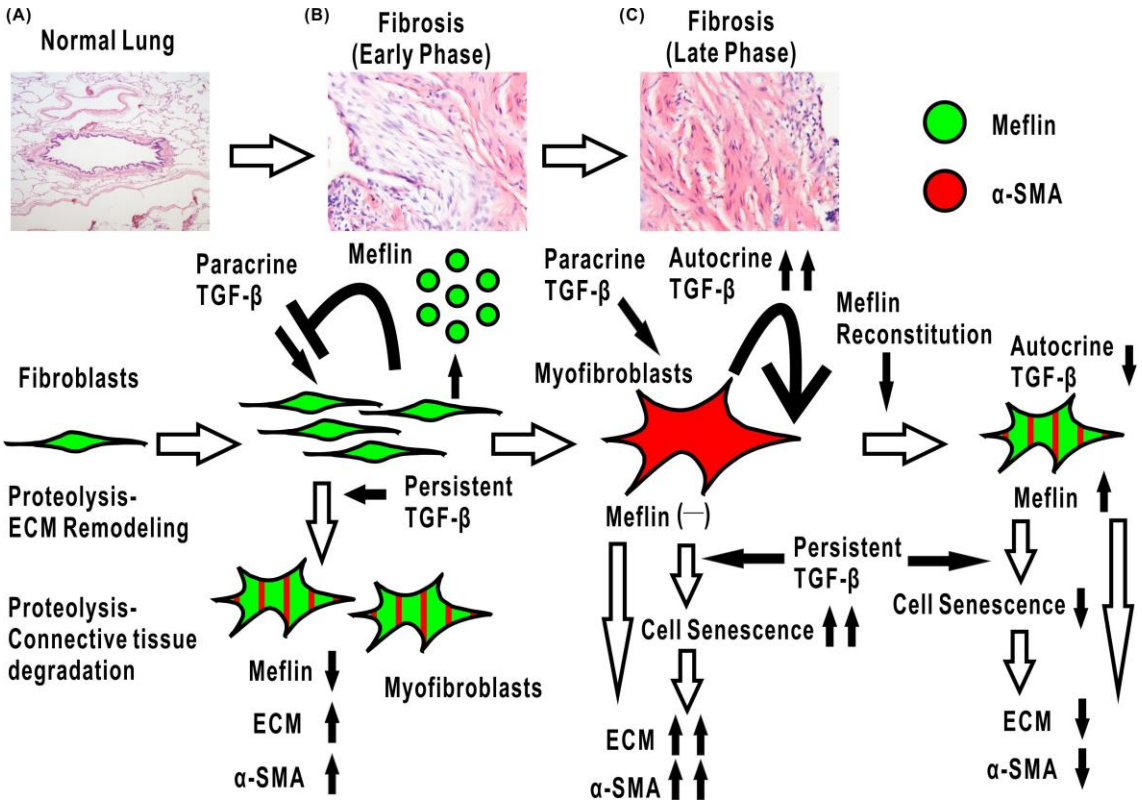

Figure 6. ***A schematic diagram of anti-fibrotic role of meflin expression on fibroblasts during development of pulmonary fibrosis***

(**A**) In normal lungs, fibroblasts positive for meflin are sporadically distributed in perivascular region or periepithelial region to control ECM homeostasis. (**B**) In early fibrotic phase, increasing meflin-positive fibroblasts inhibit TGF-β induced fibrogenesis via secretion of meflin. Persistent TGF-β stimulation cause loss of meflin expression in fibroblasts and consequently acquisition of *de novo* α-SMA expression and ECM production. (**C**) In late fibrotic phase, the lack of or repression of meflin in fibroblasts yielded TGF-β-induced cellular senescence with a senescence-associated secretory

phenotype, accompanied by exacerbation of TGF-β-induced fibrogenesis. Reconstitution of meflin expression in myofibroblasts inhibit TGF-β induced fibrogenesis and cell senescence.

Fibroblasts positive for meflin have anti-fibrotic property in pulmonary fibrosis

Yoshio Nakahara, Naozumi Hashimoto, Koji Sakamoto, Atsushi Enomoto, Taylor S. Adams, Toyoharu Yokoi, Norihito Omote, Sergio Poli, Akira Ando, Keiko Wakahara, Atsushi Suzuki, Masahide Inoue, Akitoshi Hara, Yasuyuki Mizutani, Kazuyoshi Imaizumi, Tsutomu Kawabe, Ivan O. Rosas, Masahide Takahashi, Naftali Kaminski, Yoshinori Hasegawa

Supplemental data

Materials and methods

Materials

Rabbit polyclonal anti-mouse meflin (ISLR) antibody was purchased from Atlas Antibodies (Bromma, Sweden). Purified anti-fibronectin antibody (clone TV-1) was purchased from Santa Cruz Biotechnology Inc. (Santa Cruz, CA). Mouse anti-α-smooth muscle actin (α-SMA) antibody (clone 1A4) was purchased from Lab Vision Corporation (Fremont, CA). Affinity-isolated rabbit anti-actin antibody and DNase I were purchased from Sigma-Aldrich (St. Louis, MO). ViraPower Lentiviral Packaging Mix, Lipofectamine 2000, Antibiotic-Antimycotic, and Alexa Fluor 555 goat anti-mouse IgG were purchased from Thermo Fisher Scientific, Inc (Waltham, MA). Can Get Signal was purchased from Toyobo Co. (Tokyo, Japan). PhosSTOP and liberase TM were purchased from Roche Applied Science (Mannheim, Germany). Bleomycin (BLM) was purchased from Nippon Kayaku (Tokyo, Japan). qPCR Lentivirus Titration Kit was from Applied Biological Materials Inc (Richmond, Canada). Lentivirus Concentrator Solution was from Clontech (Mountain View, CA). SA–β-gal staining kit, rabbit monoclonal anti-phospo-Smad2 (pSmad2) antibody, and mouse monoclonal anti-Smad2 antibody were from Cell Signaling Technology (Danvers, MA). Premix WST-1 cell proliferation assay system was from Takara Bio (Shiga, Japan). GoTaq 1-Step RT-qPCR System was from

Promega (Madison, WI). Recombinant TGF-β1 was from PeproTech Inc (Rocky Hill, NJ). Diff-Quick was from Sysmex Corporation (Kobe, Japan). RNAscope 2.5 HD Detection kit, RNAscope 2.5 Duplex Detection Kit, and the RNAscope Multiplex Fluorescent Reagent Kit v2 were from Advanced Cell Diagnostics, Inc. (Minneapolis, MN). Sircol soluble collagen assay kit was purchased from Biocolor life science assays (Carrickfergus, UK). The Purified Mouse Anti-E-Cadherin was from BD Biosciences (Franklin Lakes, NJ). Ponceau S Staining Solution was from Beacle. Inc. (Kyoto, Japan)

Cells and mice

293FT cells were purchased from Thermo Fisher Scientific, Inc. (Waltham, MA). 293FT cells stably expressing mouse Islr and human ISLR were utilized as previously reported [1]. A normal human lung fibroblasts (NHLF; Catalog #:CC2512) and Human lung microvascular endothelial cells (HMVEC-L; Catalog #: CC-2527) were purchased from Lonza (Lonza, Walkersville, MD, USA). Human adenocarcinoma A549 cell line and mouse lung epithelial cells (MLE12 cells) were purchased from American Type Culture Collection (Manassas, VA, USA). Human bronchial epithelial cells (HBEC-4KT) were prived from the Hamon Center collection (University of Texas Southwestern Medical Center, Dallas, TX, USA) [2, 3]. Human peripheral blood mononuclear cells (PBMC)

were isolated from whole blood by Vacutainer CPT tube (#1). The cells were cultured in Dulbecco's modified Eagle's medium (DMEM), supplemented with 2 mmol/L L-glutamine, antibiotic-antimycotic, and 10% FCS. C57BL/6J (WT) mice were obtained from Charles River Laboratories Japan (Yokohama, Japan). Meflin-deficient mice were previously generated [1]. All animal studies were reviewed and approved by the University Committee on Use and Care of Animals at Nagoya University Graduate School of Medicine (Approval date: March 22, 2019; Approval#: 31333).

Vectors and gene transfection

Mouse Meflin (Islr) cDNA obtained from Open Biosystems (clone ID. 3966024) was subcloned into a lentiviral expression vector, pLV-CMV-Ash-MCL-Puromycin vector (pLV-mMeflin) (Medical & Biological Laboratories Co., Ltd, Nagoya, Japan) [1]. A pLV-CMV-Azami-Green-MCL-Neomycin vector (Medical & Biological Laboratories Co., Ltd, Nagoya, Japan) was utilized as a control vector (pLV-AG). After transduction of pLV-mMeflin into primary fibroblasts as below for 24 hours, the culture medium was replaced and incubated for another 24 hours prior to treatment with TGF-β1. Human Meflin (ISLR) cDNA was subcloned into a lentiviral vector, pLV[Exp]-Puro-CMV>hISLR [NM_201526.2](pLV-hMeflin) (VectorBuilder Inc, Chicago, IL). A

pLV[Exp]-Puro-CMV>EGFP vector (VectorBuilder Inc, Chicago, IL) was used as a control vector (pLV-EGFP). After transduction of pLV-hMeflin into normal human lung fibroblasts (NHLF) for 24 hours, the culture medium was replaced and incubated for another 24 hours prior to treatment with TGF-β1. NHLF were treated with TGF-β1(5 ng/ml) for 72 hours. The lentiviral titers were determined by the qPCR Lentivirus Titration Kit and the adequate multiplicity of infection (MOI) for primary fibroblasts was determined according to the manufacturer's instructions. The DNA recombination experiments in this study were carried out in compliance with the guidelines of Nagoya University Graduate School of Medicine and approved by the Nagoya University Center for Gene Research (Approval date: July 16, 2019; Approval#: 19-21).

Analysis of microarray data of human samples

Microarray data available at the GEO (Gene Expression Omnibus) (www.ncbi.nlm.nih.gov/geo/) functional genomics data repository hosted by the NCBI (National Center for Biotechnology Information). We analyzed data set GSE47460 - GPL14550 for ISLR transcript levels in normal lungs and lungs of IPF patients. Log2-transformed normalized expression values for ISLR gene in 122 IPF lungs and 91 control lungs were retrieved using GEO2R and visualized using GraphPad Prism Version 7

(GraphPad Software, San Diego, CA).

Sample preparation for single cell sequencing

IPF lungs were obtained from patients undergoing transplants while healthy lungs comprised rejected donor lung organs that underwent lung transplantation at the Brigham and Women's Hospital or donor organs provided by the National Disease Research Interchange (NDRI). The study protocol was approved by the Partners Healthcare Institutional Board Review (IRB Protocol # 2011P002419). Tissue was mechanically and enzymatically digested and single cell suspension was obtained and stored until analysis. A detailed explanation of the collection, processing, and quality control of samples described herein has been described [4]. Single cells were barcoded using the 10x Chromium Single Cell platform (3', v2); cDNA libraries were prepared according to the manufacturer's protocol. cDNA libraries were sequenced on a HiSeq 4000 Illumina platform with an average of 180.1 (±36.7) million reads per library, and an average return of 2,933 (±1,811) cells per library.

Data processing, normalization, and visualization

Reads were trimmed using Cutadapt (v-1.17) to remove template-switch oligo or polyA

contaminants. Further read processing was performed with zUMIs (v 2.0), with reads aligned to GRCh38, Ensembl release 91. Downstream normalization and analysis was conducted in R (v 3.6.1), using the Seurat (v 3.1.1) package. UMIs were normalized to 10,000 UMIs per cell, then log transformed with a pseudocount of 1 (i.e. log((TranscriptPerMillion/100)+1)). No endogenous control genes were used. The top 2,500 variable genes were selected for principle component analysis with Seurat's 'FindVariableGenes' implementation and the 'vst' selection parameter. The first 45 principle components were used for the final Uniform Manifold Approximation and Projection (UMAP) dimension reduction and clustering, with a neighborhood size of 50 cells. The same principle component and neighborhood parameters were used for Louvain clustering using the Seurat 'FindNeighbors' and 'FindClusters' implementations. Similar clusters were collapsed into major cell fractions representative of epithelial (EPCAM+), endothelial (CDH5+), immune (PTPRC+), and two mesenchymal populations (PDGFRB+ and PDGFRB high [hi]). Spearman’s correlation between ISLR expression and all other genes was conducted for both control and IPF PDGFRB+ cells using R's 'cor.test' implementation; p-values were adjusted by false discovery rate using the R 'p.adjust' implementation.

Sample preparation in the CHILDREN registry

Human lung tissue samples from 10 patients with IPF and 5 subjects with normal lungs were obtained via surgical lung biopsy or remnants of lung resection at Nagoya University Hospital. All study subjects were enrolled in the CHILDREN registry (the CHronic Interstitial Lung Disease REgistry of Nagoya University), which were approved by the Nagoya University Ethics Committee (Approval date: December, 20, 2018; Approval#:2017-0169-3). The pathological findings of usual interstitial pneumonia (UIP) pattern were determined by a chest pathologist (T.Y.) who had 30 years' experience. To determine the findings of fibroblastic foci and dense fibrosis lesions in the tissue specimens, the slides with H-E staining from 10 patients with IPF were independently reviewed by one chest pathologist (T.Y.) and three pulmonologists (N.H., K.S., and Y.N.). Information about patient characteristics, laboratory findings, the findings of chest thin-section computed tomography (TSCT), and spirometric variables was obtained from the hospital records as previously reported [5, 6].

Mouse fibrosis model

Pulmonary fibrosis was induced by endotracheal BLM injection as previously described [7, 8]. Briefly, BLM was suspended in sterile saline at 3 mg/ml. Mice were treated with 4 or 6 μg/g body weight of BLM diluted in sterile saline or the same volume of sterile

saline only. The day of the BLM administration was designated as BLM day 0 [7, 8].

Collection of mouse lung samples and bronchial alveolar lavage fluid (BALF)

At the indicated time, bronchoalveolar lavage (BAL) fluid and lung specimens were collected for further analysis [9, 10]. Separately, the lungs were fixed with 10% neutral-buffered formalin after removing the lung tissues from the thoracic cavity and cleared any extraneous tissue. For Western blotting and real-time PCR analysis, lung tissue samples were also preserved by snap-freezing.

Isolation of primary fibroblasts

Lung fibroblasts were isolated from lung tissue by mincing and enzymatic digestion using liberase and DNase I with minor modification [7, 11, 12]. After filtration, released cells were centrifuged, washed, and cultured in DMEM supplemented with 15% FCS and Antibiotic-Antimycotic. Cultured fibroblasts in this study were used for experiment between passages 1 to 2. Cells were treated with TGF-β1 (5 ng/mL) for the indicated period after passage [11, 12].

Preparation of conditioned medium containing meflin

293FT cells or 293FT cells stably expressing mouse Islr (5×10^6 cells/10cm dish) were seeded and the conditioned medium was harvested from these cells 48 hours later. Each conditioned medium was centrifuged at 2000 rpm × 20 minutes and the supernatants were harvested. The presence of meflin in the culture supernatant was confirmed by Western blot and Ponceau S staining. MLE-12 cells and primary lung fibroblasts from meflin KO mice were treated by each culture supernatant and administered simultaneously with TGF-β1 for the indicated period. MLE-12 cells and primary lung fibroblasts were treated with TGF-β1 (10 ng/ml) for 72 hours and TGF-β1 (5 ng/ml) for 48 hours, respectively.

In situ hybridization (ISH)

As previously reported [1, 13], all ISH analyses were performed on formalin-fixed and paraffin-embedded human and mouse tissue samples using RNAscope 2.5 HD Detection Kit for detection of one gene or RNAscope 2.5 Duplex Detection Kit for detection of two genes, according to the manufacturer's instructions. Staining was visualized with 3,3'-diaminobenzidine (DAB) or Fast Red, followed by counterstaining with hematoxylin. For detection of one gene, staining was visualized with 3,3'-diaminobenzidine (DAB), followed by counterstaining with hematoxylin. To detect the expression of two genes, the hybridization of two probes were visualized by red and green chromogens, followed by

counterstaining with hematoxylin. RNAscope probes used in the study were human meflin (ISLR) (NM_005545.3, region 275–1322, catalog number 455481 or 455481-C2); mouse meflin (Islr) (NM_012043.4, region 763-1690, catalog number 450041); and human ACTA2 (NM_001613.2, region 10-1341, catalog number 311811); negative control probe (DapB) (EF191515, region 414-862, catalog number 312038); positive control probe (Hs-UBC) (NM_021009, region 342-1503, catalog number 312028). The proportion of fibroblasts with substantial meflin (red) and/or α-SMA (green) signal dots was quantified in at least three microscopic fields of fibroblastic foci and dense fibrotic lesions in the lungs from IPF patients (x200 magnification) [14, 15]. For each evaluation, the number of mRNA-positive cells that co-localized with nuclei were manually counted and divided by the total number of fibroblasts in each lesion.

Dual in situ hybridization (ISH)-immunohistochemistry (IHC) staining

Dual ISH-IHC analyses were performed using formalin-fixed and paraffin-embedded human IPF lung samples to detect meflin mRNA and E-cadherin [16]. In brief, the samples were incubated with RNAscope probe of human meflin (ISLR) (NM_005545.3, region 275-1322; catalog number 455481) and visualized using the RNAscope Multiplex Fluorescent Reagent Kit v2 (Advanced Cell Diagnostics, catalog number 323100)

according to the manufacturer's instructions. On the same slides, E-cadherin was subsequently detected by IHC using the Purified Mouse Anti-E-Cadherin and Alexa Fluor 555 goat anti-mouse IgG.

Senescence-associated β-galactosidase (SA-βgal) staining

Primary lung fibroblasts from WT and meflin KO mice (1.0×10^5 cells/well) were seeded in 6-well plates and treated with TGF-β1 for the indicated period. SA–βgal staining was performed using a SA–βgal staining kit according to the manufacturer's instructions as previously described [17]. Culture plates were captured at x100 magnification and senescent cells were identified as blue-stained cells under light microscopy. Total numbers of cells were counted in 3 random fields on a slide to determine the percentage of SA–βgal–positive cells.

Real-time PCR

Total RNA was isolated from treated cells as previously described [18, 19]. Real-time PCR assays were performed using the GoTaq Probe 1-Step RTqPCR System (Promega, Madison, WI) with a TaqMan ABI 7300 Sequence Detection System (PE Applied Biosystems, Foster City, CA). These mRNA expression levels were normalized to the

18s rRNA mRNAs signals [20]. The oligonucleotide primers are shown in Table S3.

Western blotting analysis

For lung tissues and whole-cell extracts, samples were harvested in ice-cold lysis buffer and cleared by centrifugation [9, 21-23]. The samples were then subjected to SDS-PAGE and analyzed by immunoblotting; β-actin was evaluated as a loading control. After scanning the film to create a digital image, the amount of protein on the immunoblots was quantified by Quantity One image software (BioRad Laboratories, Philadelphia, PA) [12, 22].

Collagen content assay

The acid soluble collagen was quantified for mouse lung homogenate samples, fibroblasts lysates, and conditioned medium collected from mouse fibroblasts, MLE-12 cells, and NHLF, using Sircol soluble collagen assay kit [24]. The largest lobe of right lung was obtained for this assay. Primary lung fibroblasts from WT and meflin KO mice (2.0×10^5 cells/well) were seeded in 6-well plates and treated with TGF-β1 for 72 hours. Conditioned medium and cell lysates were respectively harvested from these cells. The collagen samples were measured at a 555-nm wavelength as a manufacture instruction.

Cell proliferation assay

Primary lung fibroblasts from WT and meflin KO mice (1.0×10^4 cells/well) were seeded in 96-well plates and treated with TGF-β1 for the indicated period. WST-1 cell proliferation assay was performed as described previously [25]. OD values were divided by the OD value of day 0 for normalization, and fold increase was used to evaluate cell proliferation. Primary lung fibroblasts from WT and meflin KO mice (1.0×10^5 cells/well) were seeded in 6-well plates and treated with TGF-β1 for 72 hours. Cells were trypsinized, and the number of cells were counted by TC20 Automated Cell Counter (Bio Lad, Hercules, CA) at day 0 and day 3, and fold increase was calculated. The assays were performed in triplicate.

Statistical analysis

Data were presented as median ± range when specified. Comparison of two groups was performed using unpaired Student's t-test (parametric) or Mann- Whitney U-test (non-parametric). For multiple comparison, we used a repeated measures ANOVA with post-hoc Bonferroni's test or a one-way ANOVA with post-hoc Tukey's test to determine the significance. Kaplan-Meier survival estimation with a log-rank test was performed to

compare the animal survival rate between treatment groups. All statistical analyses were performed using SPSS statistical software (IBM Corp, Chicago, IL). A value < 0.05 was considered statistically significant.

Supplemental references

1. Maeda K, Enomoto A, Hara A *et al*. Identification of Meflin as a Potential Marker for Mesenchymal Stromal Cells. Sci Rep 2016; 6:22288.
2. Ramirez RD, Sheridan S, Girard L *et al*. Immortalization of human bronchial epithelial cells in the absence of viral oncoproteins. Cancer Res 2004; 64(24):9027-9034.
3. Tanaka I, Sato M, Kato T *et al*. eIF2beta, a subunit of translation-initiation factor EIF2, is a potential therapeutic target for non-small cell lung cancer. Cancer Sci 2018; 109(6):1843-1852.
4. Chu SG, Poli De Frias S, Sakairi Y *et al*. Biobanking and cryopreservation of human lung explants for omic analysis. Eur Respir J 2020; 55(1).
5. Hashimoto N, Iwano S, Kawaguchi K *et al*. Impact of Thin-Section Computed Tomography-Determined Combined Pulmonary Fibrosis and Emphysema on Outcomes Among Patients With Resected Lung Cancer. Ann Thorac Surg 2016; 102(2):440-447.
6. Hashimoto N, Ando A, Iwano S *et al*. Thin-section computed tomography-determined usual interstitial pneumonia pattern affects the decision-making process for resection in newly diagnosed lung cancer patients: a retrospective

study. BMC Pulm Med 2018; 18(1):2.

7. Hashimoto N, Jin H, Liu T *et al*. Bone marrow-derived progenitor cells in pulmonary fibrosis. J Clin Invest 2004; 113(2):243-252.

8. Hashimoto N, Phan SH, Imaizumi K *et al*. Endothelial-mesenchymal transition in bleomycin-induced pulmonary fibrosis. Am J Respir Cell Mol Biol 2010; 43(2):161-172.

9. Hashimoto N, Kawabe T, Imaizumi K *et al*. CD40 plays a crucial role in lipopolysaccharide-induced acute lung injury. Am J Respir Cell Mol Biol 2004; 30(6):808-815.

10. Shibasaki M, Hashimoto K, Okamoto M *et al*. Up-regulation of surfactant protein production in a mouse model of secondary pulmonary alveolar proteinosis. Am J Respir Cell Mol Biol 2009; 40(5):536-542.

11. Nakamura T, Matsushima M, Hayashi Y *et al*. Attenuation of transforming growth factor-beta-stimulated collagen production in fibroblasts by quercetin-induced heme oxygenase-1. Am J Respir Cell Mol Biol 2011; 44(5):614-620.

12. Kimura M, Hashimoto N, Kusunose M *et al*. Exogenous induction of unphosphorylated PTEN reduces TGFbeta-induced extracellular matrix expressions in lung fibroblasts. Wound Repair Regen 2017; 25(1):86-97.

13. Hara A, Kobayashi H, Asai N *et al*. Roles of the Mesenchymal Stromal/Stem Cell Marker Meflin in Cardiac Tissue Repair and the Development of Diastolic Dysfunction. Circ Res 2019; 125(4):414-430.

14. Kwon S, Chin K, Nederlof M *et al*. Quantitative, in situ analysis of mRNAs and proteins with subcellular resolution. Sci Rep 2017; 7(1):16459.

15. Villapol S, Loane DJ, Burns MP. Sexual dimorphism in the inflammatory response to traumatic brain injury. Glia 2017; 65(9):1423-1438.

16. Li H, Courtois ET, Sengupta D *et al*. Reference component analysis of single-cell transcriptomes elucidates cellular heterogeneity in human colorectal tumors. Nat Genet 2017; 49(5):708-718.

17. Debacq-Chainiaux F, Erusalimsky JD, Campisi J *et al*. Protocols to detect senescence-associated beta-galactosidase (SA-betagal) activity, a biomarker of senescent cells in culture and in vivo. Nat Protoc 2009; 4(12):1798-1806.

18. Nakashima H, Hashimoto N, Aoyama D *et al*. Involvement of the transcription factor twist in phenotype alteration through epithelial-mesenchymal transition in lung cancer cells. Mol Carcinog 2012; 51(5):400-410.

19. Ando A, Hashimoto N, Sakamoto K *et al*. Repressive role of stabilized hypoxia inducible factor 1alpha expression on transforming growth factor beta-induced

extracellular matrix production in lung cancer cells. Cancer Sci 2019; 110(6):1959-1973.

20. Sakamoto K, Hashimoto N, Kondoh Y *et al*. Differential modulation of surfactant protein D under acute and persistent hypoxia in acute lung injury. Am J Physiol Lung Cell Mol Physiol 2012; 303(1):L43-53.

21. Aoyama D, Hashimoto N, Sakamoto K *et al*. Involvement of TGFbeta-Induced Phosphorylation of the PTEN C-Terminus on TGFbeta-Induced Acquisition of Malignant Phenotypes in Lung Cancer Cells. PLoS One 2013; 8(11):e81133.

22. Kusunose M, Hashimoto N, Kimura M *et al*. Direct regulation of transforming growth factor beta-induced epithelial-mesenchymal transition by the protein phosphatase activity of unphosphorylated PTEN in lung cancer cells. Cancer Sci 2015; 106:1693-1704.

23. Kohnoh T, Hashimoto N, Ando A *et al*. Hypoxia-induced modulation of PTEN activity and EMT phenotypes in lung cancers. Cancer Cell Int 2016; 16:33.

24. Chung KP, Hsu CL, Fan LC *et al*. Mitofusins regulate lipid metabolism to mediate the development of lung fibrosis. Nat Commun 2019; 10(1):3390.

25. Shuda M, Kwun HJ, Feng H *et al*. Human Merkel cell polyomavirus small T antigen is an oncoprotein targeting the 4E-BP1 translation regulator. J Clin

1 Invest 2011; 121(9):3623-3634.

2

3

Supplemental Figure Legends

Figure S1. ***Single Cell RNAseq analysis of ISLR expression in human lung scRNAseq data***

(**A)** UMAPs of 243,472 cells from control and IPF lungs, showing classical cell markers for immune (PRPRC), epithelial (EPCAM), endothelial (CDH5), and mesenchymal (PDGFRB) cell populations. The expression of COX4I2 (**B**), MCAM (**C**), ACTG2 (**D**), and DES (**E**), are shown as violin plot. The PDGFRB hi/EPCAM-/CDH5-/PTPRC- group, defined as pericytes with COX4I2, MCAM, ACTG2, and DES expressions, showed no or little ISLR expression. **(F)** Heatmap of scaled gene expression amongst ISLR-high cell populations across subjects from controls or IPF. The top 80 genes ranked by p-value from a Spearman's correlation test with ISLR expression are shown. (**G**) Results of gene enrichment analysis using Genego Metacore software. Top 10 'Process networks' with the top 400 genes ranked by p-value from a Spearman's correlation test with ISLR expression in PDGFRB+ cells from normal controls (top; Cont) and IPF lungs (bottom; IPF) were shown with -log10 FDR (false discovery rate).

Figure S2. ***Analysis of ISLR expression profiles in single cell resolution using user-friendly web database***

ISLR expression profile in single cell resolution was visualized by "Idiopathic Pulmonary Fibrosis Cell Atlas" (http://ipfcellatlas.com), web-based datamining tool for sc-RNA seq datasets published in the recent publications/preprints describing the result of sc-RNA seq data of human lung cell samples. UMAP plots describing the distribution of ISLR expressing cells in clusters of different lineages including all samples were drawing by UMAP Explorer, and violin plots visualizing ISLR expression in each cell type stratified by disease states are drawn by Gene Explorer. (**A**), (**B**), (**C**): Kropski's dataset; (**D**), (**E**), (**F**): Lafyatis's dataset; (**G**), (**H**), (**I**): Misharin's dataset. The labellings of each cell cluster are shown in (**A**), (**D**), and (**G**). ISLR relative expression in each dataset is shown in (**B**), (**E**), and (**H**). Violin plots showing ISLR expression stratified by disease status of cell origin are shown in (**C**) from Kropski's dataset, and (**F**) from Lafyatis's dataset respectively. (**I**) The box-whisker plot indicating average ISLR expression by subject, stratified by disease status of cell origin.

Figure S3. ***Fibrotic variables mRNA expression in lung tissues from healthy subjects and patients with idiopathic pulmonary fibrosis.***

The expression of FN1 (**A**), ACTA2 (**B**), and COL1A1 (**C**) transcripts were evaluated in lung homogenates from IPF (n = 10) and control (n = 5) lungs among subjects

enrolled in the CHILDREN study. *P < 0.05 in comparison with control group. The expression of ISLR (**D**) transcripts were evaluated in lung fibroblasts derived from IPF (n = 5) and control (n = 3) lungs among subjects enrolled in the CHILDREN study. *P < 0.05 in comparison with control group. H-E staining (**E**) was performed for representative lung sections from control group (case 189). X40 magnification. The lined box area and dotted box area indicate perivascular region and periepithelial region, respectively. H-E staining (**F** and **H**) were performed for representative lung sections from the IPF group. (**F**) X100 magnification. (**H**) X200 magnification. Combined staining of the ISH for ISLR (red) and the immunohistochemistry (IHC) for E-cadherin (green) and nucleus (blue) were also performed for the serial section (**G** and **I**). Scar bars indicate 50μm in (**G**) and 100μm in (**I**), respectively. Yellow arrows indicate epithelial cells positive for E-cadherin. Yellow arrow heads indicate fibroblasts positive for ISLR. The expression of ISLR (**J**) transcripts and meflin protein expressions (**K**) were evaluated in several human cells. HBEC4-KT; human bronchial epithelial cells: A549; Human adenocarcinoma cell line: NHLF; normal human lung fibroblasts (CC2512): HMVEC-L; human lung microvascular endothelial cells: PBMC; human peripheral blood mononuclear cells. NC: cell lysate of 293FT cells. PC: cell lysate of 293FT cells stably expressing human ISLR. (**A**)-(**D**): Mann–Whitney U-

test. (**J**): a one-way ANOVA with post-hoc Tukey's test. The experiment was repeated three times with similar results.

Figure S4. ***ISLR mRNA expression in lung tissues from healthy subjects and patients with idiopathic pulmonary fibrosis***

Lung tissues from healthy subjects (case 186) were evaluated by H-E staining (**A**), the ISH for DapB as negative control (**B**), Hs-UBC as positive control (C), ISLR (red) and ACTA2 (green) (**D**); X40 magnification. The dotted box area in (**A**) indicates periepithelial region. For the dotted area, H-E staining (**E**) and the ISH for DapB as negative control (**F**), Hs-UBC as positive control (G), ISLR (red) and ACTA2 (green) (**H**), were shown; X200 magnification. Fibrotic foci region (**I**-**P**) and dense fibrosis region (**Q**-**X**) of lung tissues from IPF patient (case 209) were also evaluated by H-E staining (**I and Q**; X40 magnification: **M** and **U**; X200 magnification), the ISH for DapB as negative control (**J and R**; X40 magnification: **N** and **V**; X200 magnification), Hs-UBC as positive control (**K** and **S**; X40 magnification: **O** and **W**; X200 magnification), ISLR (red) and ACTA2 (green) (**L** and **T**; X40 magnification: **P** and **X**; X200 magnification). The dotted box area in (**I**) and (**Q**) were evaluated in (**M**)-(**P**) and (**U**)-(**X**), respectively.

Figure S5. ***Pathological evaluation in lung tissues from patients with idiopathic pulmonary fibrosis***

Lung tissues from IPF patients were evaluated by H-E staining (**A**: case 171; **B**: case 184; **C**: case 192; **D**: case 193; **E**: case 197; **F**: case 201; **G**: case 202; **H**: case 205; **I**: case 207; **J**: case 209, respectively); X20 magnification. Each dotted box area in Figure S5 was evaluated in Figure S6.

Figure S6. ***ISLR mRNA expression in lung tissues from patients with idiopathic pulmonary fibrosis***

H-E staining (left panel) and the ISH for ISLR (red) and ACTA2 (green) (right panel) were perform for lung tissues from IPF patients (**A**: case 171; **B**: case 184; **C**: case 192; **D**: case 193; **E**: case 197; **F**: case 201; **G**: case 202; **H**: case 205; **I**: case 207; **J**: case 209, respectively); X100 magnification.

Figure S7. ***Anti-fibrotic effect of meflin-positive fibroblasts in an in vivo BLM-induced lung fibrosis model***

Realtime PCR analyses for Fn1 (**A**), Acta2 (**B**), Col1a1 (**C**), Tgfb1 (**D**), Il1b (**E**), and

Tnfa (F) were performed for lung homogenates from saline-treated wild (WT) mice (**close square**) and BLM-treated WT mice (**open square**) collected at the indicate time. *P < 0.05 in comparison with D0. Lung tissues from saline-treated (**G-J**) and BLM-treated (**K-N**) mice were evaluated by H-E staining (**G** and **K**), the ISH for DapB as negative control (**H** and **L**), the ISH for ISLR (brown) (**I** and **M**). The lined box area in (**G**) and dotted box areas in (**K**) indicate periepithelial region and fibrotic region, respectively. For the lined box area in (**G**), the ISH for ISLR (brown) were shown. For the dotted box area in (**K**), the ISH for ISLR (brown) were shown. Original magnification: X200 for (**G**)-(**I**) and (**K**)-(**M**); X400 for (**J**) and (**N**), respectively. Islr (**O**), Tgfb3 (**P**), Postn (**Q**), Il1b (**R**), Il6 (**S**), Tnfa (**T**), Cxcl2 (**U**), Ccl2 (**V**), Ccl3 (**W**), p16INK4a (**X**), p19ARF (**Y**), and p21 (**Z**) were performed for lung homogenates from treated mice. *P < 0.05 in comparison with saline-treated WT mice. # P < 0.05 in comparison with BLM-treated WT mice. (**A-F**): a repeated measures ANOVA with post-hoc Bonferroni's test. (**O-Z**): a one-way ANOVA with post-hoc Tukey's test. The experiment was repeated three times with similar results.

Figure S8. ***Anti-fibrotic roles of meflin in primary mouse lung fibroblasts ex vivo against TGF-β-induced fibrogenesis***

Realtime PCR analyses for Islr (**A**), Fn1 (**B**), Acta2 (**C**), Col1a1 (**D**), Postn (**H**), Cxcl2 (**I**), and Ccl2 (**J**) were performed in control or TGF-β-stimulated primary lung fibroblasts from WT and KO mice. *P < 0.05 in comparison with saline-treated WT mice. # P < 0.05 in comparison with BLM-treated WT mice. Collagen content of conditioned medium collected from fibroblasts (**E**) evaluated by sircol collagen assay was shown. (**F**) The expressions of psmad2, smad2, and β-actin, were evaluated using Western blot analyses. A representative blots were shown in a left panel in (**F**). The number of cells were counted at day3 after TGF-β-stimulation (**G**). Realtime PCR analyses for Islr (**K**), Fn1 (**L**), Acta2 (**M**), Col1a1 (**N**), Postn (**R**), Cxcl2 (**S**), and Ccl2 (**T**) were also performed in control or TGF-β-stimulated primary lung fibroblasts from KO mice, for which control or meflin were reconstituted. Collagen content of conditioned medium collected from reconstituted fibroblasts (**O**) evaluated by sircol collagen assay was shown. (**P**)The expressions of psmad2, smad2, and β-actin, were evaluated using Western blot analyses. A representative blots were shown in a left panel in (**P**). The number of cells were counted at day3 after TGF-β-stimulation (**Q**). *P < 0.05 in comparison with saline-treated WT mice. # P < 0.05 in comparison with BLM-treated WT mice. (**A-T)**: a one-way ANOVA with post-hoc Tukey's test. The experiment was repeated at least three times with similar results.

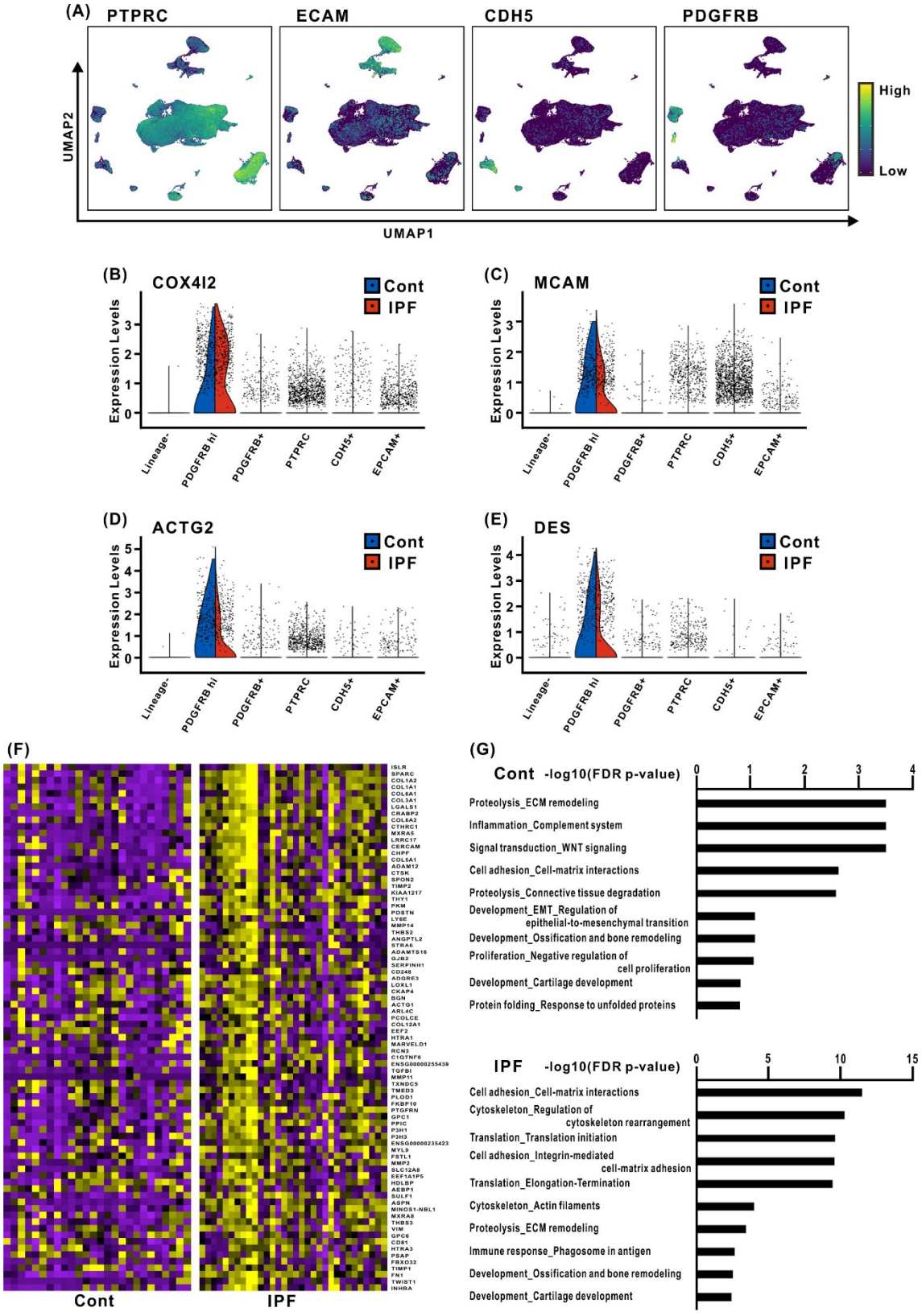

Figure S1. ***Single Cell RNAseq analysis of ISLR expression in human lung scRNAseq data***

(**A)** UMAPs of 243,472 cells from control and IPF lungs, showing classical cell markers for immune (PRPRC), epithelial (EPCAM), endothelial (CDH5), and mesenchymal (PDGFRB) cell populations. The expression of COX4I2 (**B**), MCAM (**C**), ACTG2 (**D**), and DES (**E**), are shown as violin plot. The PDGFRB hi/EPCAM-/CDH5-/PTPRC- group, defined as pericytes with COX4I2, MCAM, ACTG2, and DES expressions, showed no or little ISLR expression. **(F)** Heatmap of scaled gene expression amongst ISLR-high cell populations across subjects from controls or IPF. The top 80 genes ranked by p-value from a Spearman's correlation test with ISLR expression are shown. (**G**) Results of gene enrichment analysis using Genego Metacore software. Top 10 'Process networks' with the top 400 genes ranked by p-value from a Spearman's correlation test with ISLR expression in PDGFRB+ cells from normal controls (top; Cont) and IPF lungs (bottom; IPF) were shown with -log10 FDR (false discovery rate).

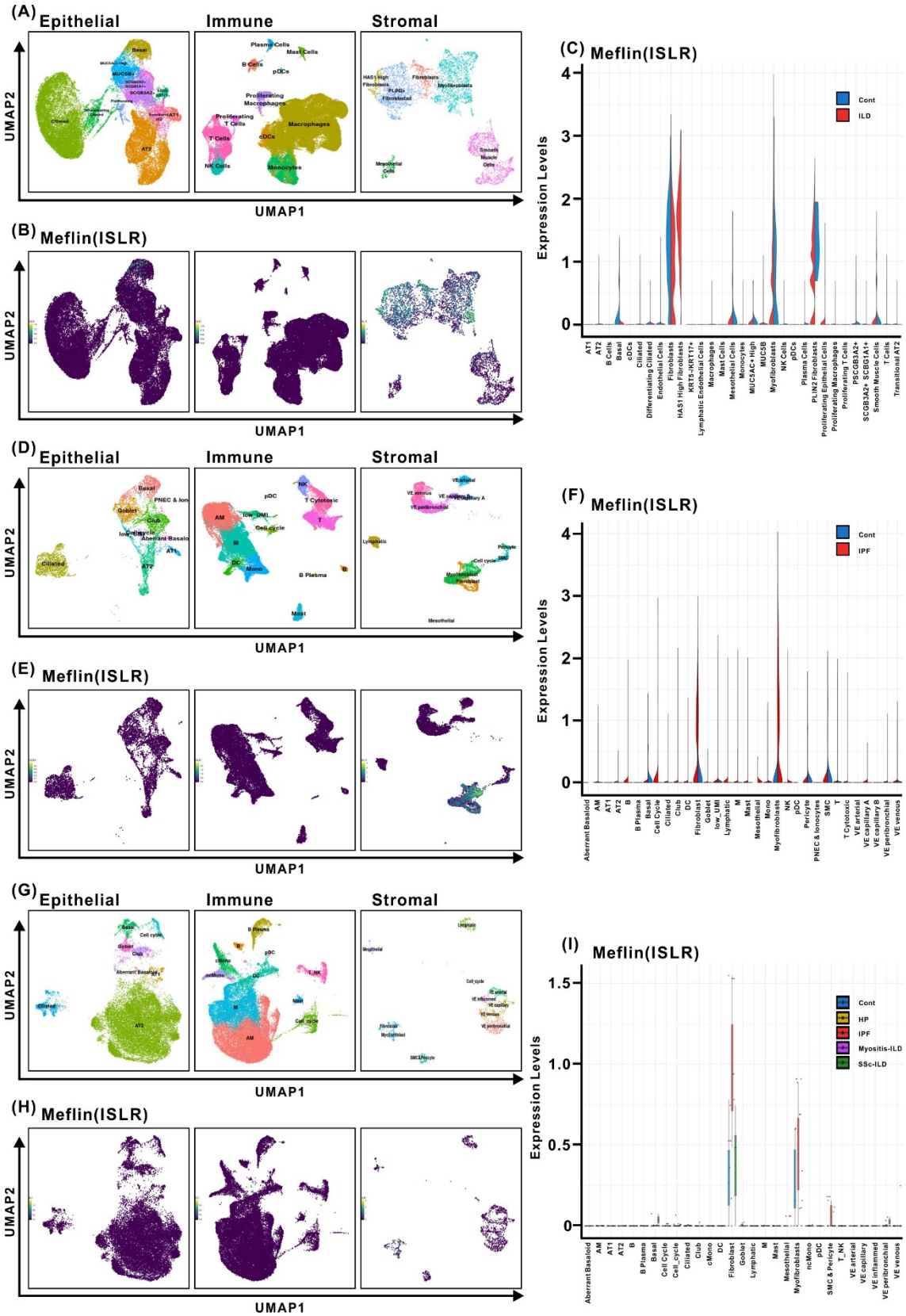

Figure S2. ***Analysis of ISLR expression profiles in single cell resolution using user-***

friendly web database

ISLR expression profile in single cell resolution was visualized by "Idiopathic Pulmonary Fibrosis Cell Atlas" (http://ipfcellatlas.com), web-based datamining tool for sc-RNA seq datasets published in the recent publications/preprints describing the result of sc-RNA seq data of human lung cell samples. UMAP plots describing the distribution of ISLR expressing cells in clusters of different lineages including all samples were drawing by UMAP Explorer, and violin plots visualizing ISLR expression in each cell type stratified by disease states are drawn by Gene Explorer. (**A**), (**B**), (**C**): Kropski's dataset; (**D**), (**E**), (**F**): Lafyatis's dataset; (**G**), (**H**), (**I**): Misharin's dataset. The labellings of each cell cluster are shown in (**A**), (**D**), and (**G**). ISLR relative expression in each dataset is shown in (**B**), (**E**), and (**H**). Violin plots showing ISLR expression stratified by disease status of cell origin are shown in (**C**) from Kropski's dataset, and (**F**) from Lafyatis's dataset respectively. (**I**) The box-whisker plot indicating average ISLR expression by subject, stratified by disease status of cell origin.

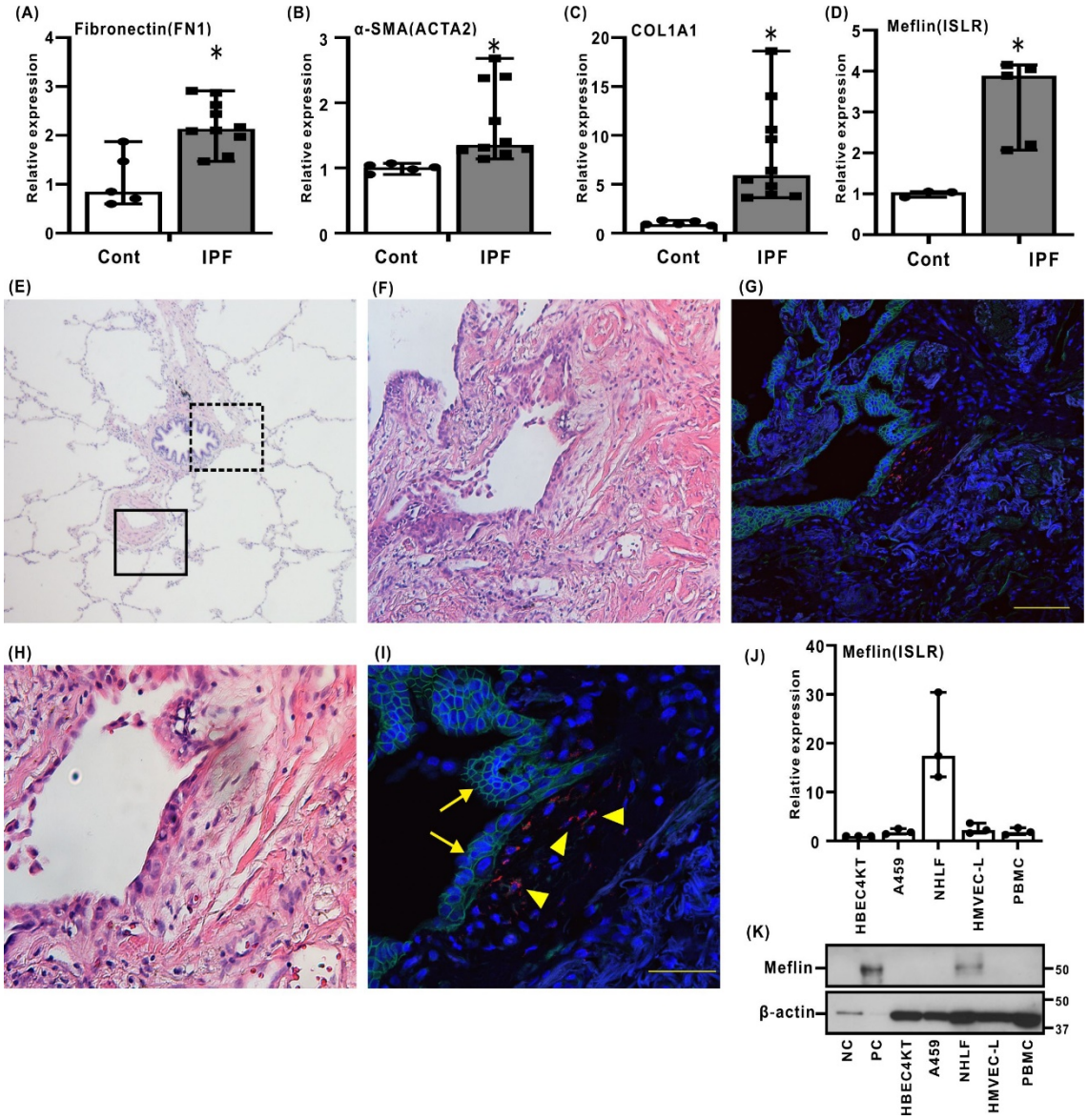

Figure S3. ***Fibrotic variables mRNA expression in lung tissues from healthy subjects and patients with idiopathic pulmonary fibrosis.***

The expression of FN1 (**A**), ACTA2 (**B**), and COL1A1 (**C**) transcripts were evaluated in lung homogenates from IPF (n = 10) and control (n = 5) lungs among subjects enrolled in the CHILDREN study. *P < 0.05 in comparison with control group. The expression of ISLR (**D**) transcripts were evaluated in lung fibroblasts derived from IPF (n = 5) and control (n = 3) lungs among subjects enrolled in the CHILDREN study. *P < 0.05 in comparison with control group. H-E staining (**E**) was performed for representative lung sections from control group (case 189). X40 magnification. The lined box area and dot box area indicate perivascular region and periepithelial region, respectively. H-E staining (**F** and **H**) were performed for representative lung sections

from IPF group. (**F**) X100 magnification. (**H**) X200 magnification. Combined staining of the ISH for ISLR (red) and the immunohistochemistry (IHC) for E-cadherin (green), and nucleus (blue) were also performed for the serial section (**G** and **I**). Scar bars indicate 50μm in (**G**) and 100μm in (**I**), respectively. Yellow arrows indicate epithelial cells positive for E-cadherin. Yellow arrow heads indicate fibroblasts positive for ISLR. The expression of ISLR (**J**) transcripts and meflin protein expressions (**K**) were evaluated in several human cells. HBEC4-KT; human bronchial epithelial cells: A549; Human adenocarcinoma cell line: NHLF; normal human lung fibroblasts (CC2512): HMVEC-L; human lung microvascular endothelial cells: PBMC; human peripheral blood mononuclear cells. NC: cell lysate of 293FT cells. PC: cell lysate of 293FT cells stably expressing human ISLR. (**A**)-(**D**): Mann–Whitney U-test. (**J**): a one-way ANOVA with post-hoc Tukey's test. The experiment was repeated three times with similar results.

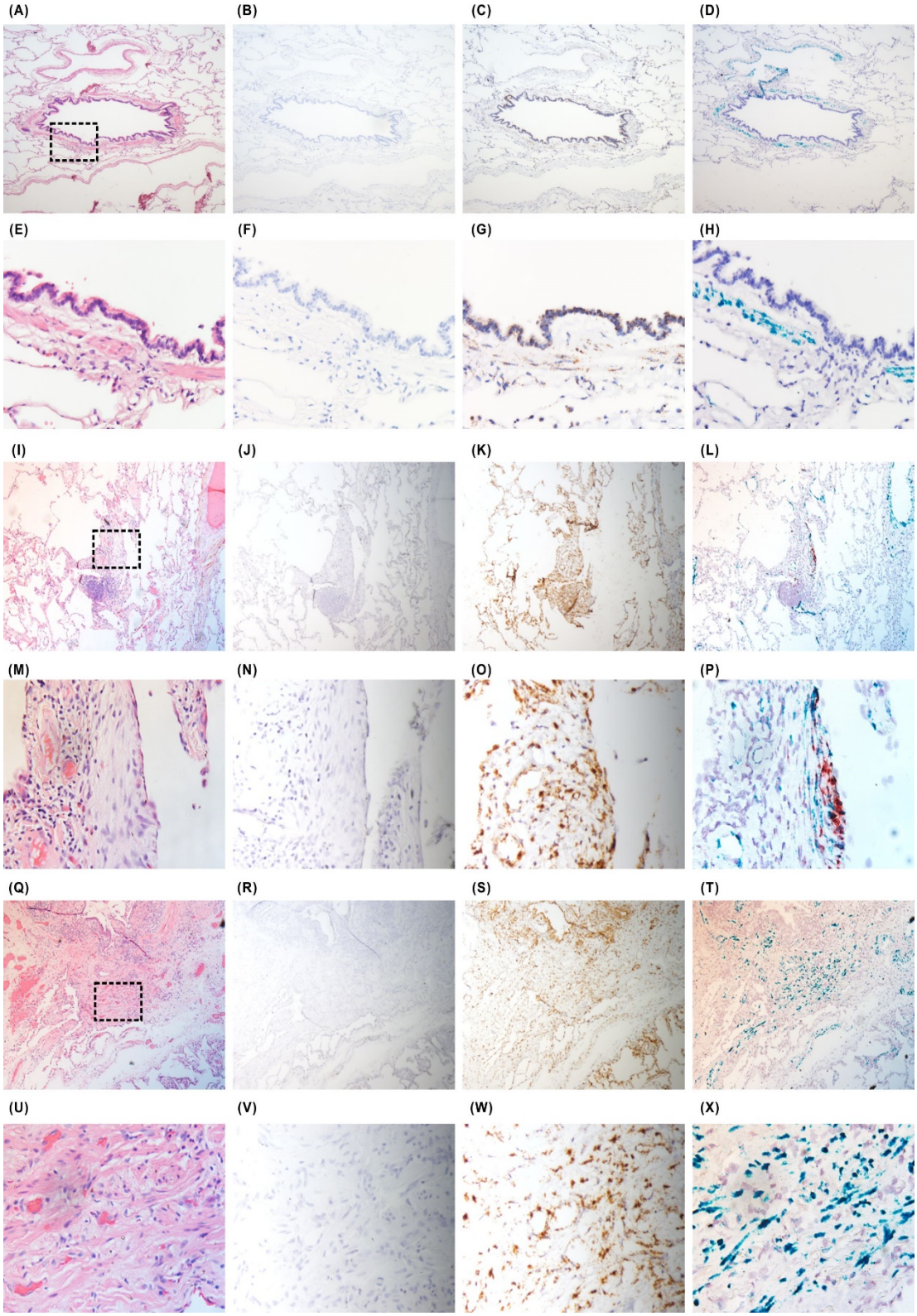

Figure S4. ***ISLR mRNA expression in lung tissues from healthy subjects and patients with idiopathic pulmonary fibrosis***

Lung tissues from healthy subjects (case 186) were evaluated by H-E staining (**A**), the

ISH for DapB as negative control (**B**), Hs-UBC as positive control (C), ISLR (red) and ACTA2 (green) (**D**); X40 magnification. The dot box area in (**A**) indicates periepithelial region. For the dot area, H-E staining (**E**) and the ISH for DapB as negative control (**F**), Hs-UBC as positive control (G), ISLR (red) and ACTA2 (green) (**H**), were shown; X200 magnification. Fibrotic foci region (**I**-**P**) and dense fibrosis region (**Q**-**X**) of lung tissues from IPF patient (case 209) were also evaluated by H-E staining (**I and Q**; X40 magnification: **M** and **U**; X200 magnification), the ISH for DapB as negative control (**J and R**; X40 magnification: **N** and **V**; X200 magnification), Hs-UBC as positive control (**K** and **S**; X40 magnification: **O** and **W**; X200 magnification), ISLR (red) and ACTA2 (green) (**L** and **T**; X40 magnification: **P** and **X**; X200 magnification). The dot box area in (**I**) and (**Q**) were evaluated in (**M**)-(**P**) and (**U**)-(**X**), respectively.

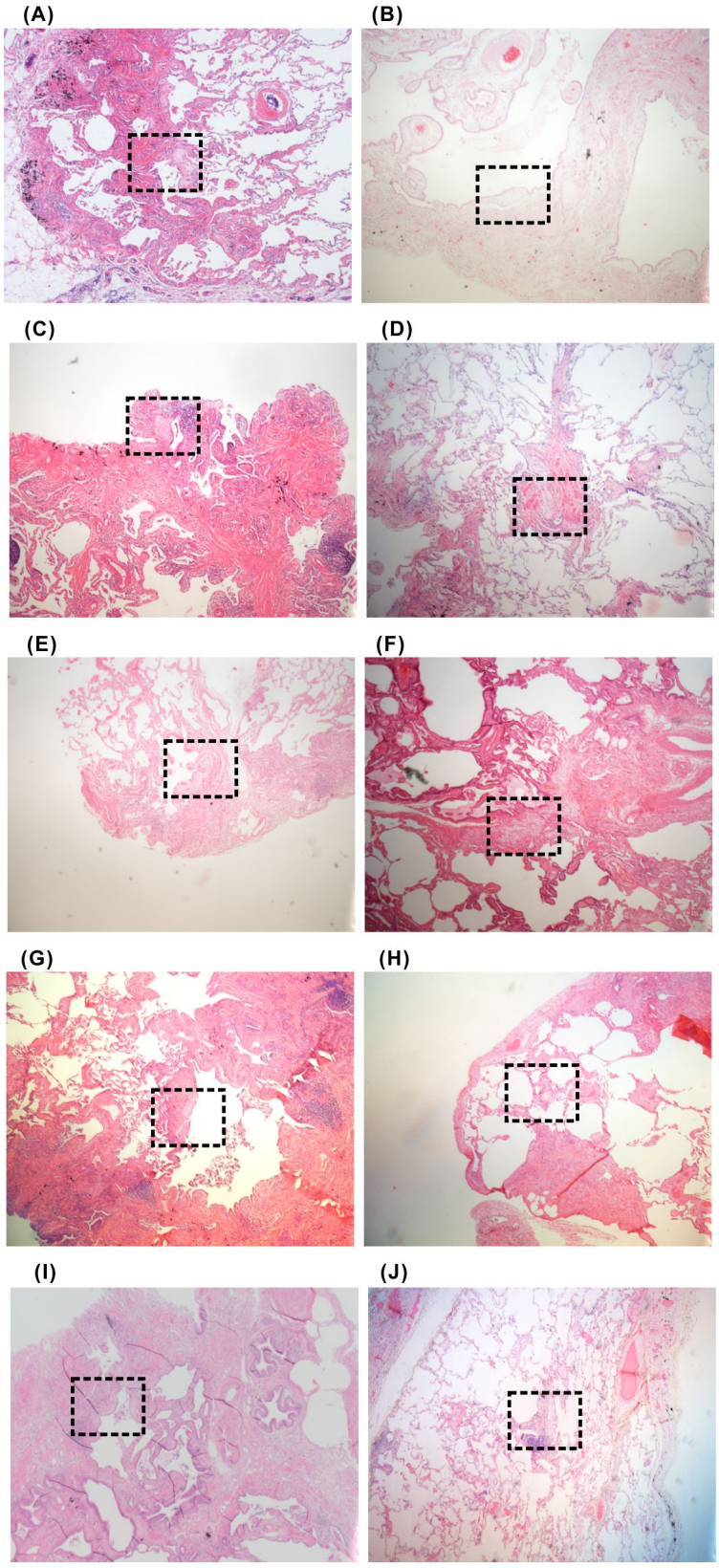

Figure S5. ***Pathological evaluation in lung tissues from patients with idiopathic pulmonary fibrosis***

Lung tissues from IPF patients were evaluated by H-E staining (**A**: case 171; **B**: case 184; **C**: case 192; **D**: case 193; **E**: case 197; **F**: case 201; **G**: case 202; **H**: case 205; **I**: case 207; **J**: case 209, respectively); X20 magnification. Each dot box area in Figure S5 was evaluated in Figure S6.

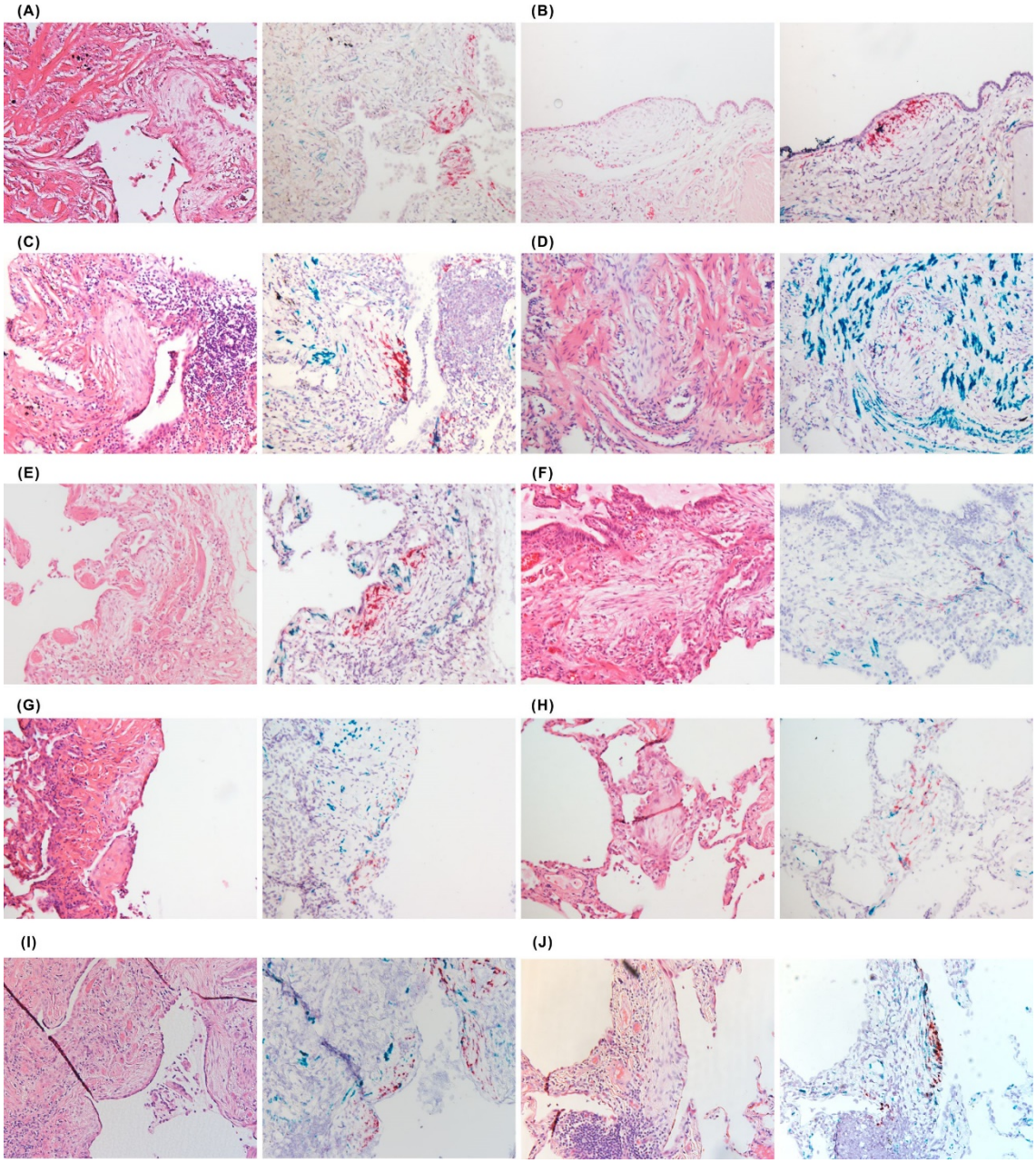

Figure S6. ***ISLR mRNA expression in lung tissues from patients with idiopathic pulmonary fibrosis***

H-E staining (left panel) and the ISH for ISLR (red) and ACTA2 (green) (right panel) were perform for lung tissues from IPF patients (**A**: case 171; **B**: case 184; **C**: case 192; **D**: case 193; **E**: case 197; **F**: case 201; **G**: case 202; **H**: case 205; **I**: case 207; **J**: case 209, respectively); X100 magnification.

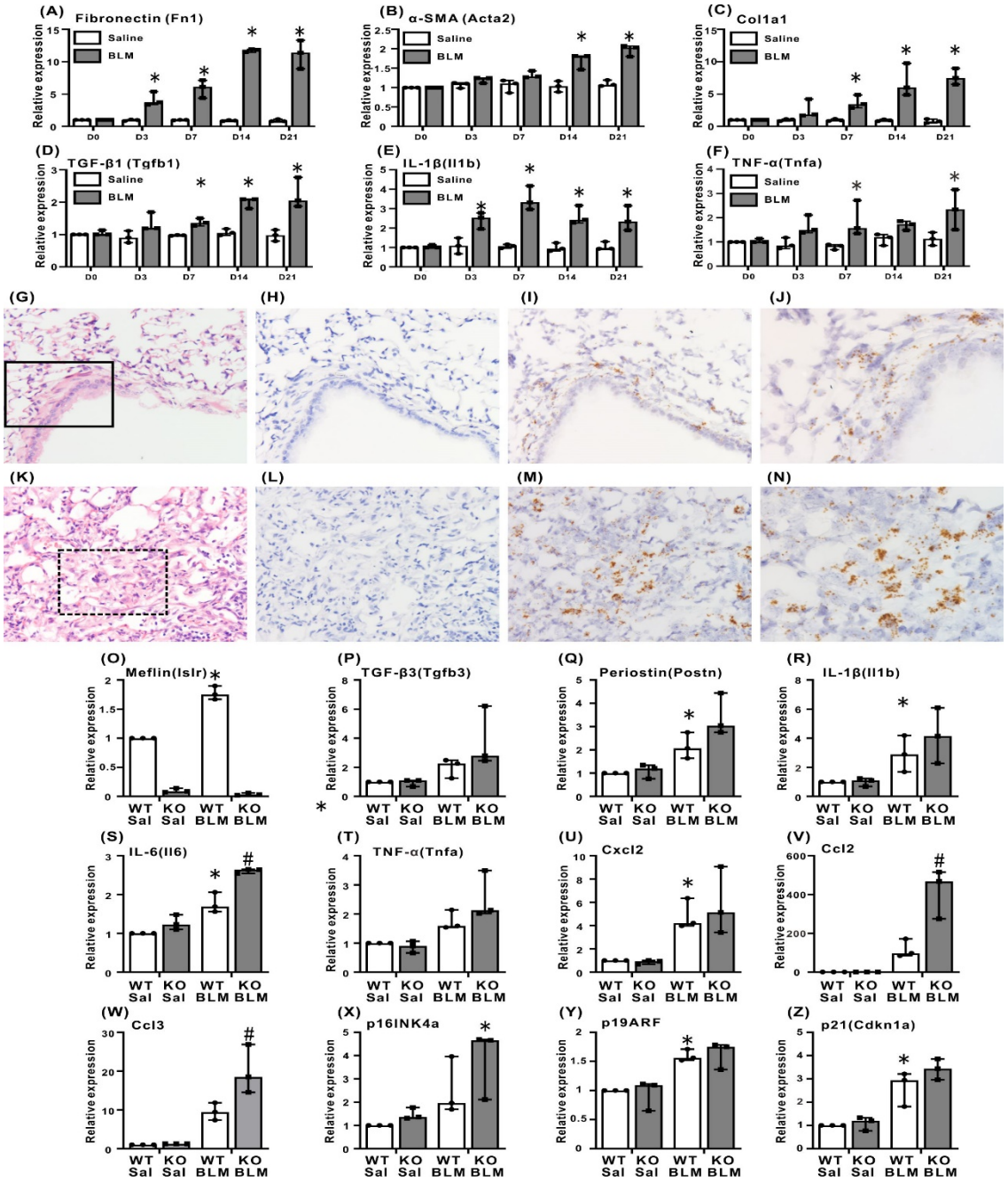

Figure S7. ***Anti-fibrotic effect of meflin-positive fibroblasts in an in vivo BLM-induced lung fibrosis model***

Realtime PCR analyses for Fn1 (**A**), Acta2 (**B**), Col1a1 (**C**), Tgfb1 (**D**), Il1b (**E**), and Tnfa (F) were performed for lung homogenates from saline-treated wild (WT) mice (**close square**) and BLM-treated WT mice (**open square**) collected at the indicate time. *P < 0.05 in comparison with D0. Lung tissues from saline-treated (**G**-**J**) and BLM-treated (**K**-**N**) mice were evaluated by H-E staining (**G** and **K**), the ISH for DapB as negative control (**H** and **L**), the ISH for ISLR (brown) (**I** and **M**). The lined box area in

(**G**) and dotted box areas in (**K**) indicate periepithelial region and fibrotic region, respectively. For the lined box area in (**G**), the ISH for ISLR (brown) were shown. For the dotted box area in (**K**), the ISH for ISLR (brown) were shown. Original magnification: X200 for (**G**)-(**I**) and (**K**)-(**M**); X400 for (**J**) and (**N**), respectively. Islr (**O**), Tgfb3 (**P**), Postn (**Q**), Il1b (**R**), Il6 (**S**), Tnfa (**T**), Cxcl2 (**U**), Ccl2 (**V**), Ccl3 (**W**), p16INK4a (**X**), p19ARF (**Y**), and p21 (**Z**) were performed for lung homogenates from treated mice. *$P < 0.05$ in comparison with saline-treated WT mice. # $P < 0.05$ in comparison with BLM-treated WT mice. (**A**-**F**): a repeated measures ANOVA with post-hoc Bonferroni's test. (**O**-**Z**): a one-way ANOVA with post-hoc Tukey's test. The experiment was repeated three times with similar results.

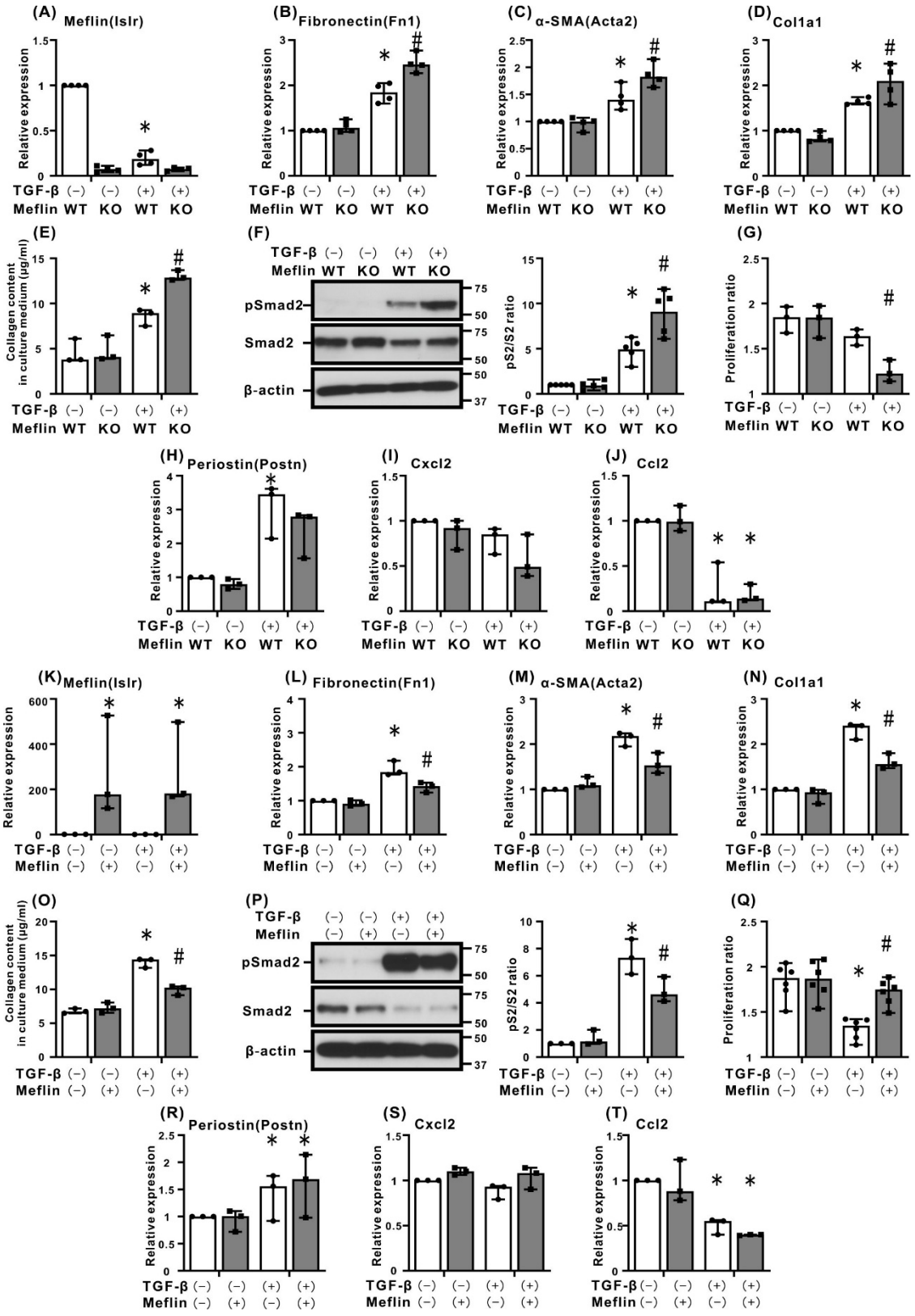

Figure S8. ***Anti-fibrotic roles of meflin in primary mouse lung fibroblasts ex vivo against TGF-β-induced fibrogenesis***

Realtime PCR analyses for Islr (**A**), Fn1 (**B**), Acta2 (**C**), Col1a1 (**D**), Postn (**H**), Cxcl2 (**I**), and Ccl2 (**J**) were performed in control or TGF-β-stimulated primary lung fibroblasts from WT and KO mice. *P < 0.05 in comparison with saline-treated WT mice. # P < 0.05 in comparison with BLM-treated WT mice. Collagen content of conditioned medium collected from fibroblasts (**E**) evaluated by sircol collagen assay was shown. (**F**) The expressions of psmad2, smad2, and β-actin, were evaluated using Western blot analyses. A representative blots were shown in a left panel in (**F**). The number of cells were counted at day3 after TGF-β-stimulation (**G**). Realtime PCR analyses for Islr (**K**), Fn1 (**L**), Acta2 (**M**), Col1a1 (**N**), Postn (**R**), Cxcl2 (**S**), and Ccl2 (**T**) were also performed in control or TGF-β-stimulated primary lung fibroblasts from KO mice, for which control or meflin were reconstituted. Collagen content of conditioned medium collected from reconstituted fibroblasts (**O**) evaluated by sircol collagen assay was shown. (**P**)The expressions of psmad2, smad2, and β-actin, were evaluated using Western blot analyses. A representative blots were shown in a left panel in (**P**). The number of cells were counted at day3 after TGF-β-stimulation (**Q**). *P < 0.05 in comparison with saline-treated WT mice. # P < 0.05 in comparison with BLM-treated WT mice. (**A-T)**: a one-way ANOVA with post-hoc Tukey's test. The experiment was repeated at least three times with similar results.

Table S1

ISLR expression in PDGFRB+ cells

Disease	# of cells	# of cells positive for ISLR	% ISLR detected	Average ISLR expression
Cont	1051	333	31.684	0.3555
IPF	4329	1827	42.204	0.5402

Cont: control; IPF: Idiopathic Pulmonary Fibrosis. # indicates number.

Adjusted bonferroni p-value: 3.170209 x 10^-08. Average natural log fold-change of 0.28 (up in IPF).

Table S2

Patient Characteristics

	Healthy Control (n=5)	**IPF (n=10)**	**P value**
Age, years*	62.2 (44-71)	65.3 (56-80)	0.562
Gender, male	60 (3)	90 (9)	0.171
History of smoking	20 (1)	90 (9)	0.007
PaO2 (Torr)	86.9 (9.4)	90.0 (9.5)	0.552
Spirometric variables			
FVC (%)**	92.5 (14.0)	90.8 (11.3)	0.797
%FEV1 predicted**	85.8 (20.0)	82.0 (11.0)	0.636
%DLCO	120.2 (17.8)	66.0 (18.9)	0.001
%DLCO/VA	114.0 (35.0)	70.6 (18.3)	0.009
KL-6 (U/ml)	NA	792.6 (390.7)	
SP-D (U/ml)	NA	250.8 (117.9)	

n indicates number. * Data are shown as mean (range). ** Data are shown as mean (standard deviation). All other data are shown as % (number). PaO2: oxygen pressure; FVC: forced vital capacity; FEV1: forced expiratory volume in the first second; DLCO: diffusion capacity for carbon monoxide; DLCO/VA: diffusing capacity of carbon monoxide by the alveolar volume; KL-6: Krebs von den Lungen 6; SP-D: Surfactant protein D.

Table S3

Sequence of the nucleotides for real-time PCR assays

Symbol/Accession		5' - 3'
18s rRNA	Forward	5'-ATCACCATTATGCAGAATCCACG-3'
NM_022551	Reverse	5'-GACCTGGCTGTATTTTCCATCC-3'
Islr	Forward	5'-GTCCTAATGTAGGCACTGATGG-3'
NM_012043	Reverse	5'-GCTTGCCAAAGTCAGGGATA-3'
Col1a1	Forward	5'-GAGGCTTCCCTGGTCTTCCT-3'
NM_007742	Reverse	5'-CTCACGTCCAGATTCACCAG-3'
Acta2	Forward	5'-CCAGCACCATGAAGATCAAGA-3'
NM_007392	Reverse	5'-CGTATTCCTGTTTGCTGATCCAC-3'
Fn1	Forward	5'-ATGTGGACCCCTCCTGATAGT-3'
NM_010233	Reverse	5'-GCCCAGTGATTTCAGCAAAGG-3'
Cdh1	Forward	5'-GCTCTCATCATCGCCACA -3'
NM_009864	Reverse	5'-GCAGTAAAGGGGGACGTGTT -3'
Tnf	Forward	5'-CCACCATCAAGGACTCAA-3'
NM_013693	Reverse	5'-CAGGGAAGAATCTGGAAAGG-3'
Il1b	Forward	5'-TGCCACCTTTTGACAGTGATG-3'
NM_008361	Reverse	5'-ATGTGCTGCTGCGAGATTTG-3'
Il6	Forward	5'-TAGTCCTTCCTACCCCAATTTCC-3'
NM_031168	Reverse	5'-TTGGTCCTTAGCCACTCCTTC-3'
Ccl2	Forward	5'-CCTGCTGCTACTCATTCACCA-3'
NM_011333	Reverse	5'-TGAGCTTGGTGACAAAAACTAC-3'
Ccl3	Forward	5'-TTCTCTGTACCATGACACTCTGC-3'
NM_011337	Reverse	5'-CGTGGAATCTTCCGGCTGTAG-3'
Cxcl2	Forward	5'-AGACAGAAGTCATAGCCACTCTCAAG-3'
NM_009140	Reverse	5'-CCTCCTTTCCAGGTCAGTTAGC-3'
Tgfb1	Forward	5'-CTGCTGACCCCCACTGATAC-3'
NM_011577	Reverse	5'-GCCCTGTATTCCGTCTCCTT-3'
Tgfb3	Forward	5'-GATCACCACAACCCACACCT-3'
NM_009368	Reverse	5'-CCAGGTTGCGGAAGCAGTAA-3'
Postn	Forward	5'-AAGTGATCCACGGAGAGCCA-3'
NM_015784	Reverse	5'-CCTGTTTCTCCACCTCCTGT-3'
p16INK4a	Forward	5'-AAGCGAACTCGAGGAGAGC-3'
NM_001040654	Reverse	5'-GTTGCCCATCATCATCACCTGAA-3'
p19ARF	Forward	5'-CGCTTCTCACCTCGCTTGTC-3'

NM_009877	Reverse	5'-CAGTGACCAAGAACCTGCGA-3'
p21	Forward	5'-CAGAATAAAAGGTGCCACAGG-3'
NM_001111099	Reverse	5'-GGGACCGAAGAGACAACGG-3'
ISLR	Forward	5'- TCAAGATGGACAGCAACGAG -3'
NM_005545	Reverse	5'- AGCGGTTGTGGTTGAGTT -3'
COL1A1	Forward	5'-GAGGCTTCCCTGGTCTTCCT-3'
NM_000088	Reverse	5'-CTCACGTCCAGATTCACCAG-3'
ACTA2	Forward	5'-CCAGCACCATGAAGATCAAGA-3'
NM_001613	Reverse	5'-CGTATTCCTGTTTGCTGATCCAC-3'
FN1	Forward	5'- GAGAATAAGCTGTACCATCGCAA -3'
NM_054034	Reverse	5'- CGACCACATAGGAAGTCCCAG -3'